Chapter 3

Mechanical Characterization of Biomaterials

Ryan K. Roeder
Department of Aerospace and Mechanical Engineering, Bioengineering Graduate Program, University of Notre Dame, Notre Dame, IN, USA

Chapter Outline

Characterization of Biomaterials. http://dx.doi.org/10.1016/B978-0-12-415800-9.00003-6

3.1. INTRODUCTION

Mechanical behavior is crucial to the performance of biomaterials used in most biomedical implants and devices. In many cases, the importance is obvious and the connection direct. The femoral stem of a total hip replacement must bear static and cyclic loads imposed by body weight and muscle forces without failure for the lifetime of the implant. In other cases, the importance of mechanical behavior is less obvious and the connection is indirect. If the aforementioned femoral stem is too stiff, cells in the adjacent bone tissue are shielded from mechanical stimuli by the implant, which can ultimately lead to implant failure via osteolysis, bone resorption, and loosening of the stem in the femur [1]. Thus, in almost all cases, including the femoral stem, *optimum device performance is predicated by optimum mechanical properties, which involves design tradeoffs*.

In other examples, middle-ear implants may preferably utilize biomaterials rigid enough to readily transmit sound waves, but ductile enough to permit intraoperative shaping [2]. A contact lens is designed to be "soft" for user comfort and is minimally loaded in use, but should not tear during repeated handling and placement [3]. Biomaterial mechanical properties may also involve spatiotemporal variations. Sutures and fixation screws used, for example, in arthroscopic reconstruction of a torn anterior cruciate ligament, may have mechanical properties that intentionally degrade over a desirable time scale after implantation [4]. Thus, *the design of biomedical devices almost always involves some form of mechanical characterization of biomaterials.*

Therefore, *the objective of this chapter is to provide a broad overview of experimental methods and important considerations for the mechanical characterization of biomaterials*. Note that the purpose here is *not* to cover the mechanical behavior of biomaterials, including structure-property relationships and deformation mechanisms. For this, the reader is referred to a welcomed new textbook focused on the mechanical behavior of biomaterials [5], and other excellent textbooks on the mechanical behavior of engineering materials [6–8]. Instead, this chapter is intended to address the practical needs of engineers and scientists who encounter a need to characterize the mechanical properties of a biomaterial, but may not know where to begin or what the key considerations should be. Of course, individuals and companies without expertise in mechanical characterization are wise to collaborate with colleagues or hire consultants who possess this expertise. However, delegation does not abdicate responsibility. The author has encountered multiple examples where a lack of basic knowledge on the part of the primary stakeholder allowed a consultant or collaborator to provide misleading or even incorrect mechanical characterization. Therefore, this chapter is also intended to be useful for those who may not perform mechanical characterization themselves.

Finally, many details are necessarily omitted from this broad overview, but references are provided to direct the reader seeking greater technical depth on

a particular topic. Of particular note, common methodologies are standardized and published by the American Society for Testing Materials (ASTM) and International Standards Organization, which provide a wealth of mechanical testing procedures and guidelines. Any laboratory or institution is wise to adopt or develop internal standard operating procedures in order to ensure the repeatability and reliability of test results, while demonstrating transparency and a mechanism for corrective measures.

3.2. FUNDAMENTAL CONCEPTS

3.2.1. Stress and Strain versus Force and Displacement

Mechanical properties of biomaterials are almost always characterized by the stresses and strains in a material that result from applied loads and displacements. Consider the schematic depiction of two different interbody spinal fusion cage designs shown in Fig. 3.1. Interbody spinal fusion cages are designed to alleviate back pain caused by a degenerated or herniated intervertebral disc by restoring the intervertebral height and facilitating the formation of bony fusion in the disc space between two vertebral bodies [9–11]. Bone formation is guided through a center cavity shown in each device.

Suppose device (1) is designed with a larger cavity in the center and a smaller cross-sectional area (A) compared to device (2), but both are composed of the same material (Fig. 3.1). If the same load (P, e.g., body weight) is applied to each device, the stress ($\sigma = P/A$) acting on the material in device (1) will exceed that in device (2), inversely proportional to the ratio of

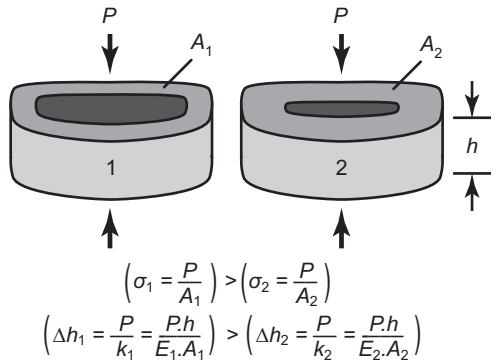

FIGURE 3.1 Differences between stress (σ) and strain (ε) versus force (P) and displacement (Δh) are introduced using the example of two interbody spinal fusion cages, where device (1) is designed with a larger cavity in the center and a smaller cross-sectional area (A) compared to device (2). For the examples described, each device has the same height (h) and the same applied load (P, e.g., body weight). The mechanics of the device, including the device stiffness (k), is shown to be governed by both the device design (e.g., A, h) and material properties (e.g., E).

cross-sectional areas (Fig. 3.1). Therefore, while it may be desirable to increase the size of the cavity for a greater fusion volume, the engineer must also consider whether greater stress in the device could result in implant failure before a fusion is achieved, or whether greater contact stress between the device with reduced cross-sectional area and adjacent bone tissue could result in subsidence of the implant into the adjacent bone tissue with loss of vertebral height [10]. On the other hand, the potentially deleterious effect of the reduced cross-sectional area on device failure can be mitigated by utilizing a material in device (1) that exhibits a greater failure strength (or stress) compared to the material used in device (2). In summary, internal stresses are related to applied loads by the inverse of the cross-sectional area (Fig. 3.1).

Deformations are also related to the applied load and cross-sectional area, as well as the material's stiffness. The amount of elastic (recoverable) deformation (Δh) due to the applied load will also be greater in device (1) compared to (2) if composed of the same material because device (1) will exhibit a lower stiffness (k, analogous to a spring) than (2) due to the smaller cross-sectional area (A) (Fig. 3.1). Internal material strains (ε) are calculated by normalizing deformations by an initial dimension (e.g., $\Delta h/h$). Therefore, a device with reduced stiffness may be advantageous for transmitting greater osteogenic strains to the bone tissue forming within the center cavity. However, notice that a reduced stiffness could also be achieved while maintaining the same cross-sectional area in device (2) by utilizing a different material to achieve a reduced stiffness (elastic modulus, E, explained below). Thus, the mechanics of a device are governed by both the device design (e.g., A, h) and material properties (e.g., E). Moreover, from a different perspective, the above example also demonstrated that *the mechanical properties of materials should always be characterized using stress and stain, instead of force and displacement, in order to avoid the influence of specimen size and facilitate interstudy comparison*.

3.2.2. Mechanical Properties on a Stress–Strain Curve

The most fundamental mechanical properties of materials are measured from a stress–strain curve (Fig. 3.2), which is calculated from the measured load and deformation during the course of a quasistatic (time-independent) test as described above. For example, consider a simple and reproducible specimen geometry, such as a right circular cylinder or a rectangular prism, loaded in quasistatic uniaxial tension. The stress–strain curve shows that this material (e.g., a metal) exhibited three regimes of deformation (Fig. 3.2a). Elastic deformation is fully recoverable, meaning that upon unloading the specimen returns to its original size and shape (Fig. 3.2b, $\Delta\varepsilon_e$). At the yield point (y), deformation is no longer fully recoverable but plastic, including permanent or inelastic deformation. Unloading at a point in the plastic range of the stress–strain curve will result in a return to zero stress but a permanent strain

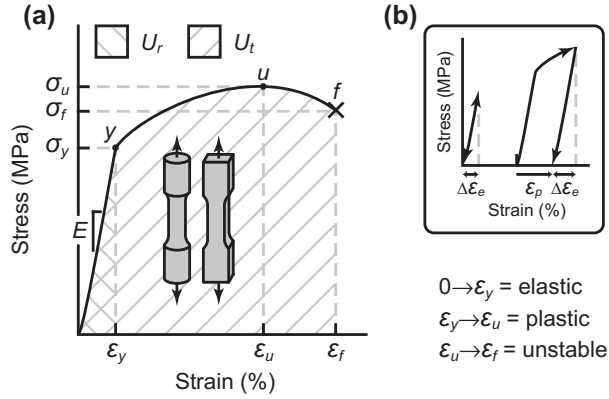

FIGURE 3.2 Schematic stress–strain (σ–ε) curves for a right circular cylinder or a rectangular prism of a material (e.g., a metal) loaded in quasistatic uniaxial tension showing (a) three regimes of deformation (elastic, plastic, and unstable) separated by critical points (y = yield, u = ultimate and f = fracture), fundamental material properties, and (b) the difference between recoverable elastic deformation ($\Delta\varepsilon_e$) and plastic or permanent deformation (ε_p). Fundamental material properties include the elastic modulus (E), yield strength and strain (σ_y, ε_y), ultimate strength and strain (σ_u, ε_u), fracture strength (σ_f), strain-to-failure (ε_f), modulus of resilience (U_r), and modulus of toughness (U_t).

(Fig. 3.2b, ε_p), typically following the slope of the elastic region. After reaching the ultimate point (u), deformation becomes unstable due to a localized reduction in cross-sectional area (necking) and fracture (f) is imminent.

The slope of the linear elastic region of the stress–strain curve ($\Delta\sigma/\Delta\varepsilon$) is termed the *elastic modulus* (E), or Young's modulus, and reflects the material's stiffness (Fig. 3.2a). Elastic moduli should be reported in units of Pa, typically GPa for most materials, although highly compliant materials such as foams and hydrogels are more conveniently reported in MPa or kPa. In polymers or ductile metals where a linear region is not readily apparent, a tangent or secant modulus may also be measured [12]. Note also that in order to facilitate accurate and repeatable measurement of strain-based properties, the presence of a "toe" region (observed as nonlinear region of increasing slope) at low stress and strain if often removed by extrapolating the measured elastic modulus to zero stress and setting strain equal to zero at that point.

The stress at the point of yielding (y) is termed the *yield strength* (σ_y or Y), and is typically reported in MPa or kPa (Fig. 3.2). Identification of the yield point is often not obvious due to a gradual transition from elastic to plastic deformation. Therefore, the yield stress is often more accurately and reproducibly measured using a line parallel to the measured elastic modulus but offset by a set amount of strain, typically 0.2% and thus termed the *0.2%-offset yield strength*. Notice that due to a phenomenon termed *strain hardening* the yield strength may be increased upon reloading a specimen previously

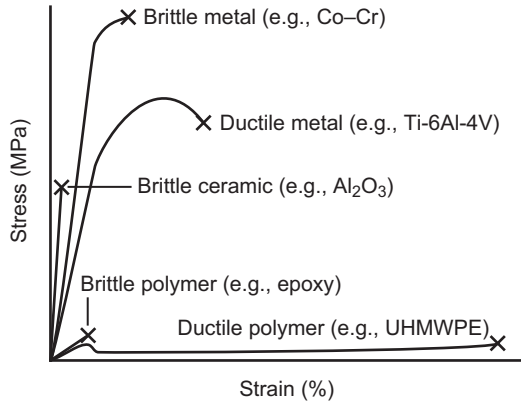

FIGURE 3.3 Schematic stress–strain (σ–ε) curves showing general differences in behavior between ceramics, metals, and polymers under quasistatic tensile loading.

plastically deformed (Fig. 3.2b). The stress at the ultimate point (u) is termed the *ultimate strength* or ultimate tensile strength (σ_u or *UTS*), and is typically reported in MPa or kPa (Fig. 3.2a). Similarly, the stress at the point of fracture (f) is termed the *fracture strength* (σ_f), and is typically reported in MPa or kPa. Note that brittle materials may not exhibit a yield or ultimate strength, but only fracture strength (Fig. 3.3).

The corresponding strains measured at the yield strength, ultimate strength, and fracture strength are termed the *yield strain* (ε_y), *ultimate strain* (ε_u), and *strain-to-failure* (ε_f), respectively (Fig. 3.2), with the latter being most commonly reported as measure of ductility. Strains are reported either in nondimensional units of the change in length divided by the original length (mm/mm), as a percentage (mm/mm $\times$ 100), or in microstrain ($\mu\varepsilon$ = mm/mm $\times$ 1000). *Ductility* is also commonly reported by the *percent elongation* (*%EL*) in tensile tests, which is the same as the percent strain-to-failure, and/or the *percent area reduction* (*%AR*), which is the percent change in cross-sectional area divided by the original cross-sectional area. *Poisson's ratio* (ν) is the negative of the ratio of a strain normal to the applied load relative to the strain in the direction of applied load. Poisson's ratio can range from $-1.0 < \nu < 0.5$ for an isotropic, linear elastic material, but is typically near 0.3 for most materials.

The area under a force–displacement curve represents the amount of work (w) to deform the material and is typically reported in N-m or N-mm; the area under the stress–strain curve represents the total *strain energy* per unit volume (U), or strain energy density, of the material, and is typically reported in J/m^3. The total strain energy up to the yield point and fracture is termed the *modulus of resilience* (U_r) and *modulus of toughness* (U_t), respectively (Fig. 3.2). While these properties provide important and useful measures of material toughness or energy absorption, they should not be mistaken or substituted as a measure of fracture toughness, which is introduced in Section 3.2.6.

3.2.3. Material Classes

The main classes of engineering materials with respect to mechanical behavior are *ceramics*, *metals*, *polymers*, and *composites* thereof. Schematic tensile stress–strain curves for examples from each class show general differences in behavior (Fig. 3.3). Under ambient and physiological conditions, ceramics typically exhibit the highest elastic modulus and high strength, but are brittle, fracturing during linear elastic deformation. Note, however, that ceramics exhibit even greater strength, by up to an order of magnitude, in compressive loading rather than tensile loading. Therefore, ceramics are typically only used in applications designed for primarily compressive stresses. Metal alloys typically exhibit a relatively high elastic modulus, the highest strength in tension, and ductility ranging from relatively brittle to highly ductile. Note that pure metals (not shown) exhibit significantly lower strength and greater ductility than metal alloys. Finally, polymers typically exhibit the lowest elastic modulus and strength. Thermoplastics (e.g., ultrahigh molecular weight polyethylene (UHMWPE)) may exhibit the greatest ductility, while thermosets (e.g., epoxy) may be stiffer and stronger, but more brittle. Composite materials exhibit properties characterized by a rule of mixtures for two or more constituent phases [13,14]. Note that all the above generalities can have exceptions. For example, ceramics can exhibit ductility at high temperature, and polymer fibers (e.g., Kevlar® or spider silk) can be prepared to exhibit extremely high strength. Nonetheless, the general *differences in mechanical properties between material classes have profound influences on the methods and analyses used for mechanical characterization*, which will become evident throughout the remainder of this chapter.

The reasons for these general differences in mechanical properties are many and a primary subject of textbooks on mechanical behavior [5–8], but a few general points are worth pointing out here. Differences in the elastic modulus and strength reflect differences in atomic bonding. In fact, mechanical properties like the elastic modulus and fracture strength can be predicted from first principles through atomistic/molecular modeling incorporating bond strengths and atomic/molecular structure [15]. The large difference in electronegativity between metal and nonmetal atoms in ceramics results in strong covalent or ionic bonding, due to electrons being shared or donated, respectively, to fill the outer shell. A small difference in electronegativity between metal atoms and excess electrons characterizes metallic bonding. However, the ductility of metals is mainly derived from crystalline defects called dislocations [5–8]. Polymers have strong covalent bonds between atoms within a molecule, but weak van der Waals bonds between molecules, which result in lower elastic modulus and strength. However, the influence of weak van der Waals bonding can be decreased and strength increased by cross-linking (thermosets) or alignment of large molecules (e.g., Kevlar® fibers or spider silk).

3.2.4. Types of Stress–Strain Curves and Constitutive Models

Stress–strain curves can take on a number of different forms including and beyond those described above (Fig. 3.4). Constitutive models of stress–strain curves are useful for characterizing the mechanical properties of materials under quasistatic loading. Constitutive models are empirical or theoretical mathematical descriptions of physical behavior. No one model is suitable for the diverse behavior exhibited by different materials under different loading conditions, but a number of common examples for quasistatic loading are shown in Fig. 3.4.

Elastic deformation is most commonly linear or approximated as linear in most metals, ceramics, polymers, and composites (Fig. 3.4a). However, elastomers and soft biological tissues like tendon may exhibit nonlinear elasticity or

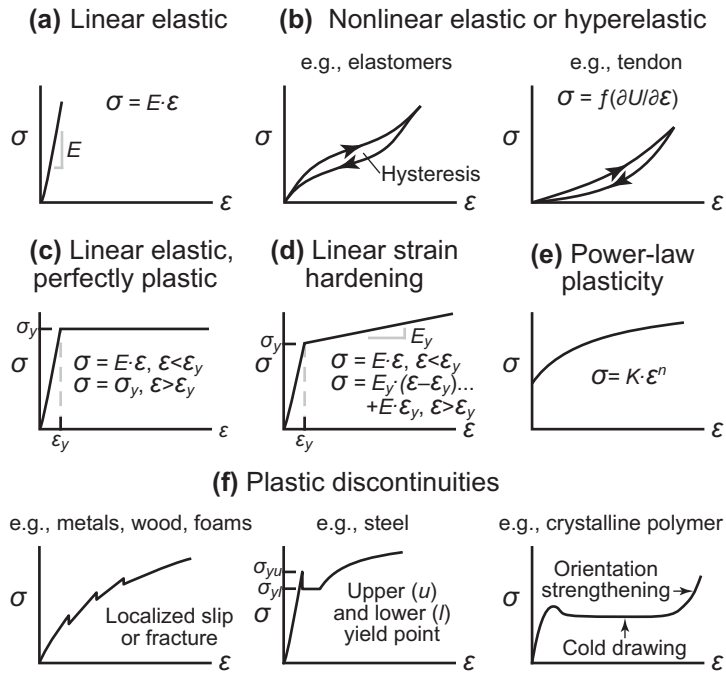

FIGURE 3.4 Common forms of stress–strain ($\sigma-\varepsilon$) curves for quasistatic loading and corresponding constitutive models for (a) linear and (b) nonlinear elastic deformation, (c) perfectly plastic deformation, plastic deformation with (d) linear or (e) power-law strain hardening, and (f) discontinuities during plastic deformation, where E is the elastic modulus, U is strain energy density, σ_y is the yield stress, ε_y is the yield strain, E_y is a "modulus" for linear strain hardening, K is the strength coefficient, n is the strain hardening exponent, σ_{yu} is the upper yield stress, and σ_{yl} is the lower yield stress. Note that all stress–strain curves are schematic and not to scale relative to each other.

hyperelasticity (Fig. 3.4b). Linear elastic deformation is readily described by Hooke's Law ($\sigma = E \cdot \varepsilon$) and its generalized form for three-dimensional deformation [6,7], while nonlinear elastic constitutive models are based on functions of the change in internal strain-energy density per change in strains [16,17].

The use of true stress and strain is an important consideration for plastic deformation that requires introduction before discussing additional constitutive models. All preceding discussions used *engineering stress and strain*, which normalized force and deformation by the *original* specimen cross-sectional area ($\sigma = F/A_o$) and length ($\varepsilon = \Delta l/l_o$), respectively. However, as noted in Section 3.2.2, plastic deformation results in permanent changes in specimen dimensions. Therefore, *true stress and strain* normalize force and deformations by the *instantaneous* specimen cross-sectional area ($\sigma = F/A_i$) and length ($\varepsilon = \ln[l/l_o]$), respectively. There is no difference between engineering and true stress/strain during elastic deformation, but during plastic deformation, and especially at large strains, true stress and strain should be used for experimental data and constitutive models. Under an assumption of volume conservation, true stress can be related to engineering stress as $\sigma_{true} = \sigma_{eng} \cdot (1+\varepsilon_{eng})$, and true strain can be related to engineering strain as $\varepsilon_{true} = \ln(1-\varepsilon_{eng})$. The assumption of volume conservation is valid for incompressible solids, which includes all relatively dense materials, but not porous materials (e.g., foams, scaffolds, and particulate compacts) where the apparent volume is not conserved during plastic deformation.

Plastic deformation may occur at a constant flow stress (Fig. 3.4c), such as during hot working of metals, or this may be used as a simplifying assumption. A strain hardening material may be modeled as linear (Fig. 3.4d), including a "modulus" for plastic deformation, or more commonly using a power-law (Fig. 3.4e). While experimental data are empirically fit by a power-law, the constants K and n are material properties with physical meaning. The strength coefficient (K) is the true stress at a true strain of one; the *strain hardening exponent* (n) is the true strain at the onset of necking or plastic instability, which corresponds to the ultimate point in engineering stress–strain (u, Fig. 3.2a).

Some materials may exhibit discontinuities in the stress–strain curve during plastic deformation (Fig. 3.4f). For example, sudden drops in stress may occur in some metals due to localized slip or dislocation motion. In steels, this behavior may be pronounced and is often characterized by an upper yield stress (σ_{yu}) and lower yield stress (σ_{yl}). Brittle materials and highly porous materials (e.g., scaffolds, foams or honeycomb structures) may similarly exhibit sudden drops in stress due to localized fracture events. This can result in "noisy" stress–strain curve data and increased error when measuring mechanical properties using the preceding constitutive models. Continuous fiber-reinforced composites often exhibit a large drop in stress coinciding with fiber failure prior to matrix failure (not shown). Finally, after an initial yield and ultimate point, semicrystalline polymers commonly exhibit extreme ductility (cold drawing) due to the unravelling and alignment of crystalline molecules (cf., Section 3.2.3), and this region

can be modeled as perfectly plastic. Orientation strengthening subsequently occurs when strong intramolecular covalent bonds begin to bear the load in place of weak intermolecular van der Waals bonds.

3.2.5. Anisotropy

Materials with directional structural features (e.g., fiber reinforcements, grain shape, crystallographic texture, etc.) exhibit anisotropic mechanical properties – that is, mechanical properties that are directionally dependent. For example, an orthotropic material exhibits three planes of symmetry such that properties differ in each of three orthogonal specimen directions. In contrast, isotropic properties are equivalent in all directions. Interestingly, engineers have historically preferred to design and use isotropic materials in man-made technology, although exceptions such a carbon fiber-reinforced plastics exist. In contrast, biological systems almost always employ anisotropic biomaterials. Bone, tendon, cartilage, tooth enamel, blood vessels, skin, wood, seashells, etc. are all composites with hierarchical and directional structural features [18,19]. The hierarchical and directional structure of natural biomaterials is critically important in enabling the biological organism to achieve the required mechanical properties while minimizing the "cost" of material mass and metabolic energy [18]. Therefore, *mechanical characterization of natural biomaterials, as well as synthetic biomaterials engineered to optimize properties and/or mimic the anisotropy of natural biomaterials, may require characterization of property anisotropy using methods described in this chapter.*

3.2.6. Fracture Mechanics

The field of fracture mechanics originated in the shipbuilding trade in the early 1900s due to a realization that engineering analysis based largely on the preceding concepts of this chapter was unable to predict prevalent catastrophic fractures of ship hulls. Cracks were observed to preferentially form around portholes and door openings due to an inhomogeneous distribution of stress, later known as a stress concentration [20]. *Stress concentration factors* are now tabulated for a number of geometric discontinuities as the ratio of a local maxima in stress at a specific geometric location relative to a nominal or remote applied stress [21]. For example, consider the addition of a circular hole to the flat specimen in Fig. 3.2 such that the size of the hole is small relative the specimen width (Fig. 3.5a). The stress concentration factor at the lateral edge of the hole is three times the remote applied tensile stress. Yet the consideration of stress concentration factors for macroscopic geometric discontinuities, while extremely important in the analysis and prediction of failure to this day, still underestimated failure. However, Inglis recognized that as the radius of curvature of an elliptical hole became increasingly sharp ($a \gg b$, Fig. 3.5a), approaching that of a sharp crack tip, the stress concentration approached infinity.

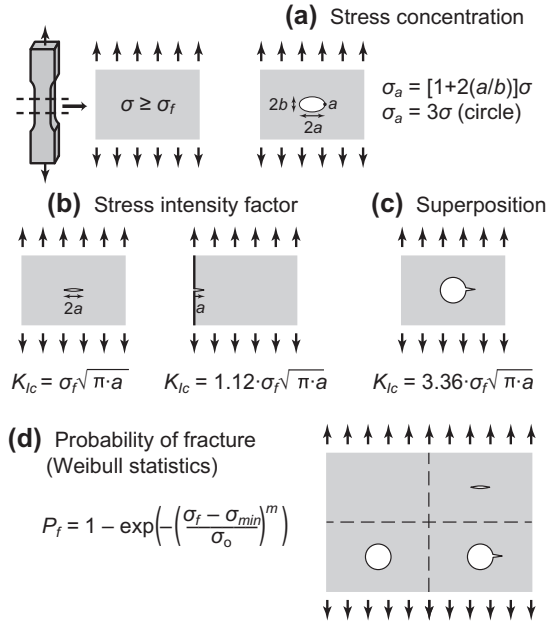

FIGURE 3.5 The development and differences between fundamental concepts in fracture mechanics beginning from a basic strength of materials analysis for a right rectangular prism of a material loaded in quasistatic uniaxial tension, including (a) stress concentrations, (b) the critical mode I stress intensity factor or plane strain fracture toughness (K_{Ic}), (c) superposition, and (d) the probability of fracture (P_f), where σ is the remote applied stress, σ_f is the fracture strength, a and b are the major and minor dimensions of an elliptical hole or crack, σ_a is the stress concentration at point a, σ_{min} is the minimum fracture strength, σ_o is a constant, and m is the Weibull modulus.

Griffith's law introduced an energy criterion for fracture based on equilibrium between the change in applied strain energy per change in crack area (energy input) and the change in surface energy per change in crack area (energy release) [22]. Therefore, catastrophic fracture occurs when crack growth is unstable due to the rate of energy input (G, termed the *strain energy release rate*) exceeding the material's ability to dissipate that energy (R, termed the *crack growth resistance*). For brittle materials, the crack growth resistance typically has a constant value or "flat R-curve." In tough materials, the crack growth resistance can increase with increasing crack length, exhibiting a "rising R-curve." Thus, one measure of a material's resistance to fracture is the *critical strain energy release rate* (G_c) for unstable crack propagation, which occurs when $dG/da > dR/da$. For example, consider the addition of a sharp elliptical through-thickness crack in the center of the flat specimen in Fig. 3.5 such that the size of the crack is small relative to the specimen width. The critical strain energy release rate for tensile (mode I) loading of a material with a flat R-curve can be derived as $G_{Ic} = (\pi \cdot \sigma_f^2 \cdot a)/E$, where σ_f is the remote applied critical stress or fracture stress, a is the crack length, and E is the elastic modulus [23].

Alternatively and more commonly, a *stress intensity factor* (K) can be used to characterize the stress field ahead of a crack tip for either crack opening (mode I), shearing (mode II), or tearing (mode III). Therefore, the fracture criterion is when K exceeds a *critical stress intensity factor* (K_c), also termed the *fracture toughness*, which is reported in units of $\text{MPa}\cdot\text{m}^{1/2}$. Note that mode I is most common and relevant since the mode I critical stress intensity factor (K_{Ic}) is typically much lower than other modes for most materials. Considering again a sharp elliptical through-thickness crack in the center of a flat specimen such that the size of the crack is small relative to the specimen width, the critical stress intensity factor, or plane strain fracture toughness, for tensile (mode I) loading is $K_{Ic} = \sigma_f \cdot (\pi \cdot a)^{1/2} = (E \cdot G_{Ic})^{1/2}$ (Fig. 3.5b). The *plane strain fracture toughness* is generalized as $K_{Ic} = Y \cdot \sigma_f \cdot (\pi \cdot a)^{1/2}$ where Y is a dimensionless geometric factor which accounts for the crack, specimen, and loading geometry such that K_{Ic} is a true material property. For an edge crack in a semi-infinite plate, $Y = 1.12$ (Fig. 3.5b). The principle of superposition can be applied to consider combinations of loading modes, cracks, and specimen geometry. For example, a simple solution for a crack at the edge of a through-thickness hole in the center of a semi-infinite flat plate is shown in Fig. 3.5c as the superposition of the stress concentration for a circular hole (Fig. 3.5a) and the stress intensity factor for an edge crack (Fig. 3.5b). Stress intensity factors for numerous geometries and standard test specimens are available in textbooks, handbooks, and ASTM standards [23–28]. Specimen requirements for a valid K_{Ic} test are described in further detail in Section 3.3.

Measurement of K_{Ic} is accomplished by loading a precracked specimen to failure while monitoring the load and displacement. A provisional fracture toughness is measured as $K_Q = P_Q \cdot f(a/W)/(B \cdot W^{1/2})$, where B is the specimen breadth and $f(a/W)$ is a dimensionless function for the ratio of the crack length (a) to specimen width (W) known for a particular specimen geometry. The crack length is typically measured directly from the specimen surface. The load at failure (P_Q) is measured from the load–displacement curve at either the first maxima encountered prior to unstable crack growth or the intersection of a secant line at 95% of the initial elastic loading slope, whichever occurs first [23,27]. If P_Q is within 10% of the maximum load measured in the test and the specimen dimensions meet the requirements detailed in Section 3.5, $K_Q = K_{Ic}$.

To summarize thus far, K characterizes local conditions near the crack tip and thus primarily governs crack initiation, while G characterizes the energetic driving force for an increment of crack extension and thus primarily governs crack propagation. Therefore, while K_{Ic} is most readily and commonly measured, the initiation fracture toughness may underestimate the true fracture toughness for tough materials that exhibit a rising R-curve. Rising R-curve behavior may be caused by a number of toughening mechanisms – including crack tip plasticity, crack deflection, crack bridging, phase transformations, and microcracking [29] – which expend strain energy for processes other than crack

propagation. In such materials, the fracture toughness during crack propagation (K_R) can be measured using displacement-controlled loading, which is amenable to stable crack propagation because unlike load control, the strain-energy release rate decreases with increased crack length. The stable instantaneous crack length is typically inferred using changes in the specimen compliance upon unloading or changes in the specimen electrical resistance, but can also be measured or confirmed directly using a traveling microscope. K_R is thus measured using similar methods to those described above for K_{Ic}, except that K_Q is measured instantaneously at multiple crack lengths, which may require plastic zone size corrections for moderate crack tip plasticity.

The preceding methods were limited to linear elastic materials, and are thus known as *linear elastic fracture mechanics* (LEFM). While LEFM can be extended to account for moderate crack tip plasticity using plastic zone size correction factors [23], tough materials exhibiting extensive crack tip plasticity or *R*-curve behavior may require the use of *elastic–plastic fracture mechanics* (EPFM). The most common EPFM methods include the measurement of a *crack-tip opening displacement* (CTOD) [30] or a nonlinear energy release rate, known as the *J-integral* [31]. A CTOD measured with an appropriate transducer (see Section 3.4.1) provides a direct assessment for the extent of crack tip plasticity in order to more accurately characterize deviation from LEFM solutions using a number of possible models. The *J*-integral assumes that elastic–plastic deformations can be idealized as nonlinear elastic and is thus analogous to *G* in practice. Therefore, J_{Ic} and *J-R* curves can be measured somewhat analogously to K_{Ic} and *K-R*, respectively, as described in detail elsewhere [23,31,32].

Fracture mechanics analyses using stress concentrations and stress intensity factors suggest that failure only requires one flaw (or crack) of a critical size and shape. However, real materials contain a statistical distribution of flaws such that a greater stressed specimen volume has a greater probability of containing a critically sized flaw and thus a greater probability of failure. This effect is most pronounced in brittle materials that are more sensitive to flaws (e.g., acrylic bone cements and ceramics), but, interestingly, has been shown to also characterize failure in "tough" biocomposites like bone [33]. *Weibull statistics* can be used to determine the *probability of failure* (P_f) using the equation shown in Fig. 3.5d, where σ_f is the fracture strength, σ_{min} is the minimum fracture strength, σ_o is a constant in units of stress, and m is the *Weibull modulus*. In the simplest method of analysis, the above parameters can be determined by a mean rank regression or other ranking methods [6,34,35]. Fracture strengths measured for each of N specimens are rank ordered and assigned integer (n) values from 1 to N. The Weibull parameter, $\log(\log(1/(1-P_f)))$, where $P_f = n/(N+1)$, is plotted versus $\log(\sigma_f)$ for each specimen. The data points are fit by a line as $m\cdot\log(\sigma_f-\sigma_{\min})-m\cdot\log(\sigma_o)$, to find the slope m and the intercept $m\cdot\log(\sigma_o)$. Thus, a relatively high Weibull modulus (m) indicates a narrow distribution of fracture strengths. Weibull analysis can be used with sample sizes as small as several specimens, but, as with any statistical

method, accuracy is improved with an increased number of specimens, especially for samples exhibiting a low Weibull modulus.

The effects of differences in specimen size and loading mode can be analyzed using more complex variations of the above analysis, which include terms for specimen volume and a nondimensional parameter called the stress-volume integral that accounts for differences in the stressed volume of a specimen for different loading modes [6,34,36]. Simplified, $<\sigma_{f1}>/<\sigma_{f2}> = (V_2/V_1)^{1/m}$, where $<\sigma_f>$ is the mean fracture strength and V is the effective stressed volume for specimens of two different geometries (1) and (2). For example, an existing data set for uniaxial tensile strength can be used to determine the probability of failure for changing the specimen size or testing the same material in three-point bending.

In summary, stress concentrations, energy criteria for crack initiation and propagation, and statistical methods for the probability of fracture were introduced as three primary methods of analysis for fracture under quasistatic loading (Fig. 3.5). Readers interested in further technical detail, including material behavior and toughening mechanisms, can readily consult numerous textbooks [5–7,23,24] on the subject matter.

3.3. SPECIMENS

3.3.1. Specimen Size and Geometry

As should be clear by now, *a standardized specimen geometry may be critical to obtaining useful test results with accurate measurements of material properties that can be compared to reference data or measurements performed by others*. To review, there are three primary reasons for this. (1) Many modes of loading result in a nonuniform stress or strain distribution within the specimen. Special considerations for common modes of loading are therefore described in Section 3.4.2 and references are provided for numerous standardized specimen geometries. (2) As described above, the stresses ahead of a crack tip in a fracture toughness test are inherently dependent on the specimen size, geometry and crack length. (3) Specimen size can influence the likelihood of encountering critically sized defects and thus the statistical distribution (Weibull modulus) of a measured material property.

Test specimens are typically prepared with a *gauge section* of reduced cross-sectional area in order to control the region of the specimen that is characterized and to provide greater surface area for gripping the specimen outside the gauge section (see Section 3.4.1). For example, extensometers or strain gauges are placed within the gauge section of tensile specimens. However, a gauge section may not be possible for all modes of loading (see Section 3.4.2).

Fracture toughness measurements require perhaps the greatest care in specimen size and geometry, and numerous standardized and nonstandardized specimen geometries are commonly utilized [23,27,28]. A valid test for K_{Ic} or

J_{Ic} requires that a, B, $(W-a) \geq 2.5(K_{Ic}/\sigma_y)^2$ or $B, (W-a) \geq 25 \cdot K_{Ic}^2/(E \cdot \sigma_y)$, respectively [27,31]. The crack length (a) and uncracked ligament length ($W-a$) criteria ensure a sufficiently small plastic zone for the implicit assumptions of each approach. The specimen breadth (B) criteria ensure plane strain conditions ahead of the crack, although the criteria in this standard have been noted to be more stringent than necessary [23]. Three-dimensional stress analysis of a crack front revealed that greater triaxiality in the specimen center results in predominate plane strain conditions and a smaller plastic zone size compared to the specimen edges where biaxial stresses (plane stress) allow shear deformation and a greater plastic zone size. True plane stress conditions exist only for infinitely thin specimens (perhaps a metal foil) and increasing specimen breadth (B) results in an increased plane strain region such that K_I asymptotically approaches a constant value (K_{Ic}), which is independent of specimen breadth.

Despite the above reasons, there can be unique situations where a standardized specimen size and geometry is simply not possible or feasible. One common example is the mechanical characterization of biological specimens (e.g., whole animal bones) possessing an inherently variable and complex size and shape, which may itself be an important consideration in the mechanical characterization. In this case, measurements may be limited to force, displacement, and stiffness, or approximations may be used to estimate stress, strain, and moduli. Despite these limitations, useful conclusions can be reached regarding biological influences (e.g., genetics [37]) on the biomaterial properties, but these conclusions must be kept within proper context. Another common example is when only a small volume of material is available, requiring deviation from standard specimen sizes [32]. In this situation, one must take special care to clearly define the measured properties, identify deviations from existing standards, and place results in an appropriate context, avoiding comparisons that are simply not valid.

3.3.2. Specimen Preparation

Test specimens are most often machined using cutting and/or grinding tools on mills, lathes, and saws. A standardized specimen size and geometry can be replicated from a computer-aided design drawing using computer numerical control machining or from a template using a pattern-following cutting tool. Care must be taken during the machining process to achieve a smooth surface finish free from defects and to prevent the specimen material from significant alterations due to the generation of heat or surface damage by cutting tools. Lubricants and cutting fluids can be used to reduce heat but must be compatible with the material. Tissue specimens should always remain fully hydrated during preparation. The cutting speed, cutting depth, tool material, and tool geometry should be appropriately selected for the material, specimen geometry, and desired surface finish. Consultation and guidelines can be sought from

experienced machinists, commercial suppliers of comparable materials, and machining handbooks [38–40].

Specimens may also be prepared by a variety of near-net-shape processes, such as injection molding plastics, that are beyond the scope of this chapter. In general, if the goal is to measure or compare material properties, care should be taken to minimize undesirable influences of the process on the material. Standards may exist for the preparation of test specimens [41,42] and textbooks on manufacturing processes describe fundamental influences [43].

The surface finish of as-machined or as-molded specimens is often inadequate for a particular material or mechanical test. Tool and die marks remaining on the surface can act as stress concentrations, which is especially problematic for brittle (flaw-sensitive) materials, flexural loading, and/or fatigue testing. Therefore, specimen surfaces, especially within the gauge section or at locations of maximum stress, are often polished using abrasives or diamond tooling of a specified grit size, and sharp corners or mold lines may be removed [28,44]. Quality test results are well worth the added labor and cost of careful specimen preparation.

Fracture toughness (Section 3.2.6) and fatigue crack propagation (Section 3.4.4.3) tests typically require the presence of a sharp crack. Various methods may be used depending on the material, specimen, and preference, but all begin with a stress concentration created by machining a notch using a diamond saw, razor blade, or electric discharge machining. A preload is subsequently applied using either a rigid fixture to "pop-in" a stable crack [28] or cyclic loading to initiate a stable fatigue crack [27]. Microhardness indentations (Section 3.4.5.1) may also be used to either directly initiate a sharp half-penny crack below the indentation or to subsequently preload as described above [28]. Grooves are also occasionally added to the sides of fracture toughness and fatigue specimens to guide crack propagation during *R*-curve and fatigue crack propagation measurements, respectively [27]. Side grooves removing no more than 20% of the specimen breadth can also act to remove the influence of plane stress conditions at the specimen surface. However, side grooves may also forcibly remove the effects of crack deflection on *R*-curve behavior and overly deep grooves can lead to decreased fracture toughness.

3.4. APPLICATION AND MEASUREMENT OF LOAD AND DEFORMATION

3.4.1. Equipment

The application of load(s) for mechanical characterization of materials is accomplished using an *actuator* with feedback to a control system (Fig. 3.6). Actuation has historically been accomplished using either a screw-driven (via an electric motor) or servo-hydraulic *load frame*; however, recent instruments have migrated towards electromechanical systems. Each has advantages and

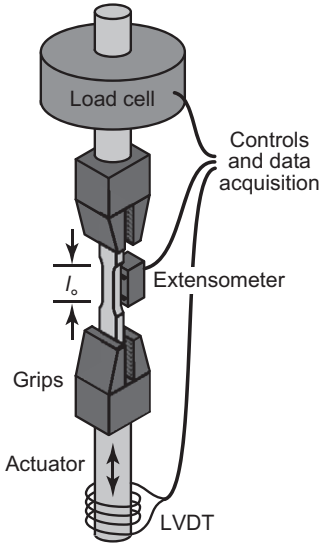

FIGURE 3.6 Schematic diagram showing a common setup for the application of load to a specimen using an actuator with feedback from transducers to a control system. Load is sensed using an in-line load cell. Actuator displacement is sensed using a linear variable displacement transducer (LVDT). Displacement within the specimen gauge length (l_o) is sensed using an extensometer or strain gauge (not shown).

limitations. Screw-driven instruments are economical but not suitable for applying high-frequency cyclic loading. Servo-hydraulic instruments are able to apply the greatest load magnitude and are well suited for cyclic loading, but typically require greater cost and maintenance. In most cases, electromechanical systems are now best suited for testing small biomaterial specimens due to their relatively high precision, adaptability, and low cost.

The applied load magnitude is sensed using an in-line *load cell* (Fig. 3.6) The most appropriate load cell for a particular application will primarily consider the load-cell capacity, sensitivity and loading mode. The load-cell capacity should not be exceeded during a test and control system shut-off switches should be set to prevent an overload. On the other hand, a load cell may be too insensitive or "noisy" at less 2% of the load-cell capacity. Load cells should be calibrated upon installation and as part of a regular maintenance schedule in order to ensure accuracy [45]. Commercial suppliers provide state-of-the-art on-site or mail-in calibration and certification against NIST traceable standards. Calibration can be readily verified by users at low cost using a set of calibration weights. Load cells may be rated for tension-only, compression-only, tension–compression, or multiaxial (axial and torsion) loading, as well as quasistatic versus cyclic loading. Finally, fully submersible load cells are also available for testing in a fluid bath.

Grips are used to transfer load from the actuator to the specimen (Fig. 3.6). The appropriate grips and gripping method are chosen to prevent slippage or failure at the grips. The most common general purpose grips clamp the specimen using a screw, a hydraulic or pneumatic piston, or a self-tightening wedge

or scissors. Slippage is prevented by increasing the clamping force and/or increasing the surface area of contact between the grip and the specimen, where the latter can be adjusted by the grip size and shape, and the use of serrated surfaces. However, an excessive clamping force, overly serrated surfaces, misaligned grips, or misaligned specimen may lead to specimen failure at the grip rather than within the specimen gauge section. Clevis pins are commonly used to grip fracture toughness specimens in order to prevent crack propagation during gripping and to allow out-of-plane rotational freedom during loading. Other specialized grips may be advantageous or necessary for testing fibers or soft materials. For example, cryogrips are useful for gripping soft, hydrated tissues such as tendon. Finally, other specialized *load fixtures* may be required for different modes of loading described in the following section.

Actuator or crosshead displacement is measured using a *linear variable displacement transducer* (LVDT) (Fig 3.6). However, the crosshead displacement includes load-line or system compliance due to the grips, specimen shoulders adjacent to the grips, couplings, load cell, etc. Load-line compliance is usually negligible in magnitude relative to the specimen compliance. However, rigid specimens and precise measurements of specimen deformation should utilize an *extensometer* to directly measure deformation within the specimen gauge length (l_o), cross-sectional area (A_o), or a crack opening. The most appropriate extensometer for a particular application will primarily consider mounting, specimen dimensions, range (or travel), and sensitivity. Contact extensometers are most common and economical, but must be carefully mounted on the specimen gauge section using clips, rubber bands, or springs. Noncontact extensometers eliminate potential influence on the specimen, and damage to the extensometer upon failure or use in extreme environmental conditions. The extensometer should be appropriately sized for the specimen dimensions. The range of a contact extensometer should not be exceeded during a test, or else the test must be paused to remove the extensometer. Moreover, the extensometer should have sufficient sensitivity within the range of displacement to be measured. Extensometers should be regularly calibrated using a micrometer in order to ensure accuracy. A limitation of an extensometer is that deformation within the specimen gauge section must be reasonably assumed to be uniform.

A *strain gauge* enables direct and highly sensitive measurement of local material strains on a specimen surface through differences in electrical resistance of a small, serpentine metal foil. The signal from a strain gauge should be measured and calibrated using a Wheatstone bridge [46]. Moreover, the gauge must be properly bonded to the specimen surface using an adhesive, such as cyanoacrylate. A strain gauge rosette can be used to determine strain directionality or principal strains on a surface. While multiple strain gauges may be used to characterize a strain field at selected points, strain gauges are not a practical means to measure nonuniform strains over a relatively large surface area. Moreover, strain gauges still require specimen contact. Popular

noncontact methods for measuring strain fields include *photoelasticity*, *digital image correlation*, and *laser interferometry*, which are described in detail elsewhere [47].

Additional information and specifications for various load frames, load cells, grips and other load fixtures, displacement transducers, extensometers, and strain gauges are readily available on the websites of companies such as Applied Test Systems, Bose Test Systems, Cooper Instruments and Systems, Epsilon, Instron, Interface, Mechanical Test Systems, Omega, Test Resources, and Vishay Precision Group, among others. A basic introduction to transducers, calibration, signal processing, and related fundamentals is also available in textbooks and handbooks [48,49].

3.4.2. Modes of Loading

A number of common loading modes may be used for different purposes described below (Fig. 3.7). Note that brittle materials (such as most ceramics, some refractory metals and hardened alloys, and some thermosetting polymers) tend to fracture along planes normal to the maximum (tensile) principal stress, even when applied loads are compressive. On the other hand, ductile materials (such as metals and thermoplastic polymers) tend deform under shear and

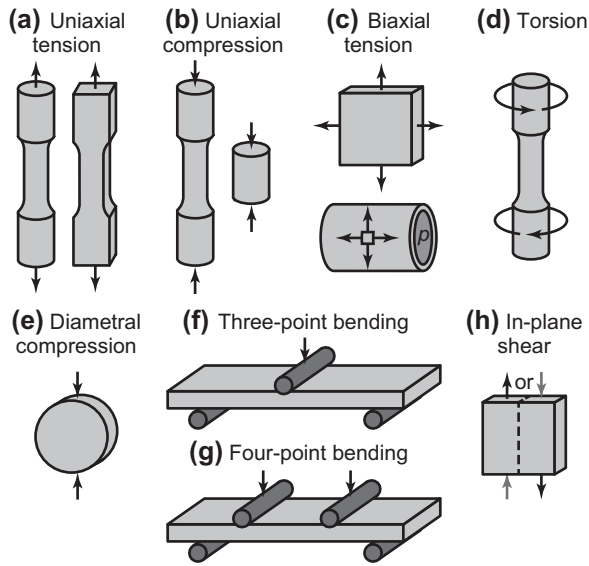

FIGURE 3.7 Common modes of loading materials for mechanical characterization include (a) uniaxial tension, (b) uniaxial compression, (c) biaxial tension, either by in-plane loading of a sheet or pressurizing (p) a vessel, (d) torsion, (e) diametral compression, (f) three-point bending, (g) four-point bending, and (h) in-plane shear.

fracture along planes of maximum shear stress. These general rules hold for all materials in all modes of loading, as described below.

Uniaxial tension (Fig. 3.7a), a.k.a., tensile testing, is the most fundamental of all tests for measuring material properties [12,50]. All preceding concepts and methods in this chapter were introduced for uniaxial tension (mode I at a crack tip) or uniaxial compression as the mode of loading. Uniaxial tension, and to a lesser extent uniaxial compression, are indeed most common and most suited for measuring material properties that are free of influences from the test method. A major reason is that the specimen cross-section experiences uniform stresses and strains. Uniaxial tension may also be useful for characterizing biomaterial-tissue interfacial strength or the bond strength between an adhesive and tissue. Microtensile bond strength is a common method for evaluating dental adhesives [51,52].

Uniaxial compression (Fig. 3.7b) is often utilized for brittle or porous materials that can be difficult to grip [42,53–55]. Moreover, brittle materials are typically designed for compressive loading in service due to exhibiting a much greater strength in compression compared to tension. Brittle materials loaded in uniaxial compression fracture at internal cone cracks. Ductile materials loaded in uniaxial compression deform by bulging at the center (termed "barreling") due to frictional stresses at the loading platens, increasing the cross-sectional area. The effects of friction and contact stresses can be minimized using highly polished loading platens, possibly with a lubricant, or by preparing specimens with a gauge section of reduced cross-sectional area, similar to tensile specimens. Porous materials (e.g., scaffolds) loaded in uniaxial compression, whether exhibiting brittle or ductile behavior, begin to densify after reaching a stress maxima or an inflection point corresponding to elastic buckling, yielding, or crushing [55,56]. Therefore, stress–strain data after this maxima and during densification are dependent on a changing level of porosity and generally not useful.

Biaxial tension (Fig. 3.7c) is particularly relevant to compliant or ductile sheet materials (e.g., skin graft, hermetic casings, and manufacturing processes for metal or polymer sheets) and thin-walled pressure vessels (e.g., the bladder, blood vessels, intravascular balloons, breast implants, etc.). Elastic and plastic deformation of materials under multiaxial loading behaves differently than under uniaxial deformation due to the effects of Poisson's ratio, yield surfaces, and possibly anisotropy. Soft tissue sheets are often gripped for planar biaxial tension through suturing [57,58], while vessels and tubes are readily loaded via internal fluid pressure [59]. Another application of biaxial loading is a *bulge test*, where a punch or applied fluid pressure is used to form a hemispherical dome in a flat sheet of a ductile material [60,61]. The utility of the bulge test lies in characterizing plastic deformation (ductility) and fracture when only a small volume of material is available due to cost or availability (e.g., implant retrieval).

Torsion (Fig. 3.7d) produces a stress state of pure shear and is thus useful for measuring material properties in shear, including nearly any that were

described above for axial loading (e.g., *shear modulus*, G). However, shear stress (τ) and strain (γ) must be treated with some caution in torsion because shear stresses and strains vary from zero at the axis of rotation to maximum values at the specimen perimeter. Torsion is particularly relevant to biomaterials used in catheters, bone screws [62], and various surgical instruments, as well as tissues [63,64]. Moreover, anisotropic properties may be characterized by combination of uniaxial tension and torsion tests [63,64]. Ductile materials loaded in torsion exhibit a flat, transverse fracture surface, while brittle materials exhibit a spiral fracture surface that is readily demonstrated with a piece of chalk.

Diametral compression (Fig. 3.7e), a.k.a., the Brazilian disk test, is perhaps a misnomer as it is used to measure the *diametral tensile strength* (*DTS*) of brittle materials as, $\sigma_{DTS} = 2P/(\pi \cdot D \cdot t)$, where D is the specimen diameter and t is the specimen thickness [65,66]. Note that the *DTS* is a surrogate for the *UTS* but is not equivalent. A proper *DTS* test specimen fails by a crack plane initiating at the center of the disk and parallel to the direction of applied load. The maximum tensile stress acts normal to the applied compressive load due to the Poisson effect. The material must exhibit sufficiently high strength and hardness such that the specimen does not permanently deform at a near-line of contact with the loading platens [66], though correction can be made to the above equation for some flattening at the contact points [67]. Diametral compression is also useful when only a small volume of material is available due to cost or availability. Biomaterial applications have included characterization of calcium phosphate cements [67] and dental cements [68].

Three-point bending (Fig. 3.7f) and *four-point bending* (Fig. 3.7g), or flexural loading, are primarily used for testing materials that are either expected to be similarly loaded in service, difficult to grip for uniaxial tension, or only available as small specimens. However, three- and four-point bendings produce multiple stress states in the specimen that are not homogeneous [5–7,69]. Portions of specimens located between the outer- and inner-loading supports are under constant shear stress/strain lengthwise, but shear stress/strain varies parabolically within the cross-section height from zero at the upper and lower surface to a maximum value at the neutral axis. For an initially flat, isotropic beam with symmetric cross-section, the neutral axis is located at the geometric centroid. Normal stress/strain increases linearly from zero at the outer load support to a maximum at the inner load support, and also from zero at the neutral axis to a maximum in tension and compression on the bottom and top specimen surfaces, respectively (Fig. 3.7f and g). Thus, for a uniform specimen cross-section, the maximum stress is $\sigma_{max} = P \cdot l \cdot h/(2 \cdot I)$, where P is the applied load, l is the distance between the outer and inner load support, h is the specimen height, and I is the cross-sectional moment of inertia (e.g., $I = b \cdot h^3/12$ for a rectangular cross-section and $I = \pi \cdot d^4/64$ for circular cross-section, where b is the specimen breadth and d is the specimen diameter). The cross-sectional distribution of maximum normal stresses remains constant within the

portion of the specimen location between the inner load supports in four-point bending.

The preceding discussion of stress analysis was necessary to highlight important considerations for flexural loading. The strength measured for a material in bending is not equivalent to that measured in uniaxial tension, and should thus be reported as the *flexural strength* or *modulus of rupture*. Moreover, even three- and four-point bending tests may exhibit differences due to the Weibull effect as the stressed specimen volume is lower in three-point bending compared to four-point bending. Thus, the strength of a material measured in three-point bending will be greater than for the same material measured in four-point bending, which is still greater than for the same material measured in uniaxial tension. The above equations, and related solutions for the elastic modulus, assume linear elastic deformation. Permanent deformation of the specimen either in bulk or due to local contact stresses at load supports can compromise the validity of measured properties and prevent the use of any stress–strain data beyond the yield point. Moreover, recall that regions of shear loading are present in the specimen. Therefore, ductile materials may undergo plastic deformation during bending even before a yield point is observed in stress–strain data. In summary, material properties measured using bending are quite sensitive to the test methods, perhaps more than any other common loading mode, highlighting the importance of the following standardized methods [44,70,71]. While there are valid reasons to use flexural tests, they should be used with caution and results should be interpreted carefully.

In-plane shear (Fig. 3.7h) is used to characterize material properties and interfaces. In-plane shear tests can be advantageous over torsion tests due to producing a reasonably uniform shear stress/strain within the specimen, but require relatively complex test fixtures and may load a relatively small volume of material. The shear properties of materials and interfaces between bulk materials can be measured using the *Iosipescu test*, *Arcan test*, *V-notch rail test* and related variations in loading fixtures and specimen geometry [72–74]. These methods were developed and are most commonly used for testing composite materials, but have also been applied to testing tissues [75].

The *biomaterial-tissue interfacial shear strength* after *in vivo* implantation is a key measurement for characterizing biocompatibility and tissue integration, particularly in load-bearing musculoskeletal tissues [76]. Several common test methods all employ in-plane shear loading to characterize the biomaterial-tissue interfacial strength. In a *push-out test*, a flat punch is used to push a biomaterial disk out of the surrounding tissue (e.g., from a cylindrical cranial, femoral, or tibial defect) using an annular fixture for the specimen. The specimen thickness and clearance (difference between the punch and annulus diameters) must be properly controlled such that failure occurs at the biomaterial-tissue interface [77]. The interfacial shear strength can be calculated by dividing the maximum load by the nominal interfacial area (cylindrical surface). Measurements are influenced by the biomaterial stiffness and should

therefore be compared only between biomaterials of similar elastic modulus [77]. In a *pull-out test*, a screw, rod, or similar biomaterial device/specimen that can be gripped is pulled out of the surrounding tissue, which must be rigidly gripped using the standard specimen grips or an annular fixture. The mechanical analysis and considerations are otherwise similar to a push-out test. However, a pull-out test can also be employed nondestructively on percutaneous devices [78]. Finally, a *torque removal test* can also be applied in similar situations as a pull-out test [62] with the load applied using torsion rather than tension.

All the above methods of loading may be applied dynamically (e.g., cyclically) in addition to quasistatic loading, as discussed in Section 3.4.4. Indentation methods of loading are discussed under nondestructive tests in Section 3.4.5.1. Mechanical characterization of *coatings* typically utilizes variants of the above methods in uniaxial tension (*pull-off test* or *peel test*), bending, or shear, and are discussed in greater detail in Chapter 4 of this book.

In summary, material properties free of the influence of test methods should be preferably measured in uniaxial tension, uniaxial compression, and (for pure shear) torsion, although other modes of loading may offer advantages relative to material properties, intended application, material form, and availability. *Therefore, material properties measured in different modes of loading should neither be treated as equivalent nor directly compared. The loading mode should always be clearly denoted when reporting material properties measured by different modes of loading.*

3.4.3. Strain Rate and Time-Dependent Behavior

The preceding methods and discussion of mechanical characterization assumed quasistatic loading and time-independent material behavior. The strain rate of a typical quasistatic mechanical test is 10^{-2} to 10^{-3} s^{-1}. However, strain rates in service may range from much higher (e.g., ~10^{2} to 10^{3} s^{-1} due to impact from a fall to ~10^{2} to 10^{6} s^{-1} due to a ballistic impact) to lower (~10^{-6}, e.g., creep under a constant load) extremes. Moreover, elastic deformation can be coupled with rate or time-dependent viscous deformation in metals and ceramics at elevated temperature, in polymers near or above the glass-transition temperature, and in hydrated tissues due to poroelasticity. Therefore, this section will overview the characterization of time-dependent mechanical behavior, including strain rate sensitivity, creep, and stress relaxation.

Differences in strain rate can profoundly influence the stress–strain behavior (and thus measured mechanical properties) for the same material in an otherwise identical test method, which is known as *strain rate sensitivity*. Strain rate sensitivity can be modeled using a power-law (similar to strain hardening in Fig. 3.4e) as $\sigma = C \cdot \dot{\varepsilon}^{m}$, where $\dot{\varepsilon}$ is the true strain rate, C is a strength coefficient, and m is the strain rate sensitivity. Note that this constitutive equation can also be coupled with the constitutive law for

power-law plasticity. The strain rate sensitivity (m) can range from 0 to 1. Most materials exhibit $m \approx 0.2$, but materials with $m > 0.3$ exhibit high strain-rate sensitivity. For example, silly putty has a strain rate sensitivity approaching the upper bound of one such that a rope of silly putty can be stretched to a nearly infinitesimally small cross-section at a low strain rate but will exhibit brittle failure when stretched at a high strain rate. Characterizing these effects in materials usually requires testing over orders of magnitude differences in strain rate.

3.4.3.1. Impact (High Strain Rates)

At increased strain rates, the effects of stress wave propagation in the specimen and acceleration on load measurement must be considered. A conventional servohydraulic or electromechanical load frame can achieve strain rates up to $10^0\ s^{-1}$, although some specialized instruments can achieve up to $10^1\ s^{-1}$. Note that the actual strain rate is dependent on the instrument crosshead speed, system compliance, specimen compliance, specimen length, and specimen cross-sectional area. Slack grips may be required to ensure that the instrument reaches the desired strain rate before loading the specimen. Moreover, the use of a conventional load cell and extensometer may be limited by inertial effects and vibrations, which can be mitigated using a stiffer piezoelectric load transducer and noncontact methods for strain measurement (Section 3.4.1).

Strain rates from 10^0 to $10^2\ s^{-1}$ can be achieved with specialized machines utilizing a pendulum or drop tower. Classic *impact testing* includes the *Charpy impact test* (or Charpy V-notch test) and *Izod impact test* [79–82]. Both tests measure the *impact energy absorption* (or "impact toughness"), typically reported in J/m or J/m^2, as a swinging mass on a pendulum strikes the specimen. The Charpy test loads a notched specimen in three-point bending, while the Izod test loads a notched specimen as a cantilevered beam. Similar impact tests can be performed using a drop tower instead of a pendulum. For example, the *Gardner test* or *free-falling dart test* is primarily used to measure the impact resistance of thin film and sheet materials [83,84]. The dart typically has a hemispherical tip, making this a dynamic punch test, but other striker tip geometries are also used. Pendulum and drop tower tests are useful for economical screening of materials (e.g., commercial quality control) and characterizing ductile–brittle transitions (e.g., due to temperature) in materials. Limitations include semiquantitative (comparative) results and a lack of strain rate control, though the strain rate can be measured with instrumentation. There has been a recent growth of interest in instrumented impact testing, as well as the development of instrumented drop weight towers, which enable high strain rate tensile testing of compliant or ductile materials at 10^1 to $10^3\ s^{-1}$ [85].

High strain rates from 10^2 to $10^4\ s^{-1}$ can be achieved using a *split Hopkinson pressure bar* (a.k.a., *Kolsky bar*), where a specimen is placed in between the ends of two straight, perfectly aligned bars called the incident and

transmitted bars [86,87]. At the end of the incident bar away from the specimen, an incident stress wave is created as the striker bar impacts the incident bar after being accelerated by a compressed gas gun. At the specimen interface, part of the stress wave is reflected back down the incident bar and another part is transmitted through the specimen and into the transmitted bar. All three bars are composed of the same material of known properties, typically a high strength steel, although softer and harder materials may be used for testing softer materials and harder materials, respectively. Strain gauges placed on the incident and transmitted bar allow the measurement of strains, strain rates, and ultimately, using known properties for the bar, a true stress–strain curve [86]. The strain rate can be controlled by varying the impact velocity (via gas pressure in the gun) and specimen size. Specimens are typically loaded in compression, although tension and torsion are also possible. Bending configurations may be used to measure dynamic fracture toughness [88,89]. Direct measurements of specimen deformation and crack growth require the use of high speed videography. While split Hopkinson bar testing is quantitative, unlike most pendulum or drop tower tests, the lack of a feedback control system typically results in an iterative design of experiments and a lack of standards. Nonetheless, split Hopkinson bar testing can be used to characterize the unique effects of high strain-rate deformation on biomaterials and tissues such as bone [89,90], which is not possible by other methods.

Very high strain rates from 10^4 to 10^6 s^{-1} can be achieved using the acceleration of projectiles or the detonation of explosives to generate shock waves [87], but are generally not relevant or necessary for biomaterials characterization.

3.4.3.2. Creep (Low Strain Rates)

At decreased strain rates, creep deformation must be considered. *Creep* is time-dependent permanent deformation under a constant stress and possibly an elevated temperature (see also Section 3.5.1), typically occurring at 10^{-3} to 10^{-8} s^{-1}. In general, all materials can exhibit creep at temperatures greater than one-third of their melting temperature, although ceramics may require a temperature closer to one-half the melting temperature, and polymers may creep at temperatures near or above their glass transition temperature. The deformation behavior in creep can be divided into three regimes after an initial elastic strain (ε_o): (1) primary or transient creep exhibiting a decreasing strain rate, (2) secondary or steady-state creep exhibiting a constant strain rate, and (3) tertiary creep or rupture exhibiting an unstable increasing strain rate preceding failure (Fig. 3.8a and b). Constitutive models for steady-state creep are useful for predicting lifetime and vary by the deformation mechanism [6–8]. Creep deformation is facilitated by a number of mechanisms including dislocation plasticity in metals, diffusion in metals and ceramics, grain

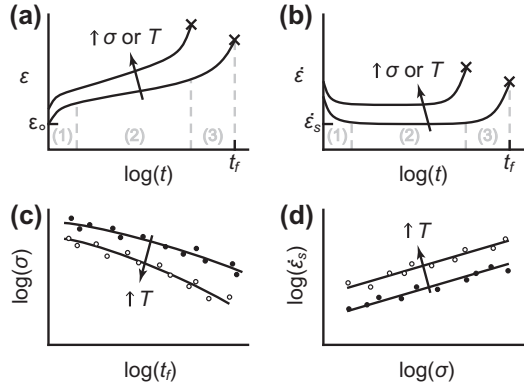

FIGURE 3.8 Schematic diagram for the time-dependent (a) strain and (b) strain rate ($\dot{\varepsilon}$) response of a material loaded under a constant stress, often at elevated temperature (T), showing three regimes of creep deformation behavior: (1) primary or transient creep exhibiting a decreasing strain rate, (2) secondary or steady-state creep exhibiting a constant strain rate, and (3) tertiary creep or rupture exhibiting an unstable increasing strain rate, preceding failure. Creep lifetime can be predicted by measuring and extrapolating (c) the creep rupture time (t_f) for accelerated tests using the Larson–Miller relation or other empirical methods, or (d) the steady-state strain rate ($\dot{\varepsilon}_s$).

boundary sliding in ceramics, and intermolecular motions (viscous flow) in viscoelastic polymers.

Superplasticity can be considered as a special case of creep deformation where a material exhibits a high resistance to necking at low strain rates (10^{-1} to 10^{-3} s^{-1}, but typically $< 10^{-2}$ s^{-1}), enabling large deformations ($\varepsilon > 1000\%$) without failure. Therefore, superplasticity is advantageous for forming of complex metallic parts as the material can exhibit Newtonian flow (viscous deformation) rather than strain-hardening plasticity and elastic recovery. In most engineering materials, superplasticity also requires elevated temperature and small, equiaxed grains.

Strain rates as low as 10^{-6} s^{-1} can be achieved using a conventional servohydraulic or electromechanical load frame. Therefore, these instruments are suitable for characterizing superplasticity in uniaxial or biaxial tension (bulge test) [91,92]. However, such an instrument is not required to apply a constant load, not to mention the impractical amount of time required for a creep test. For creep tests, a constant applied load/stress is applied using a dead weight in uniaxial tension, compression, or bending, possibly at an elevated temperature [93–95]. The strain rate is thus dependent on the specimen size, material behavior (e.g., diffusion), and influence of temperature, and must be measured by intermittent dimensional changes or *in situ*. Noncontact methods are often necessary for *in situ* strain measurements due to large deformations and/or elevated temperatures.

Given the impracticality of conducting creep rupture tests over months or years, tests are often accelerated to seconds or minutes using an increased stress

magnitude. The applied stress and *creep rupture time* (t_f) for accelerated tests can be plotted as data points on a log scale (Fig. 3.8c) and extrapolated using the Larson–Miller relation, or other empirical methods, to predict the creep rupture lifetime [6–8]. Alternatively, failure in a particular application may not require creep rupture, but only excessive deformation. In this case, the steady-state strain rate ($\dot{\varepsilon}_s$) is measured (Fig. 3.8a and b) and extrapolated either using various empirical and/or mechanistic models (Fig. 3.8d) [6–8].

3.4.3.3. Viscoelasticity

Viscoelasticity is observed as a combination of both recoverable elastic deformation and permanent viscous deformation. In the previous section, the contribution of viscous deformation was shown to result in time-dependent permanent deformation (*creep*) under an instantaneous, constant stress. Similarly, under an instantaneous constant deformation or strain, viscous deformation can cause *stress relaxation* (Fig. 3.9). Nearly all synthetic and natural polymers used as biomaterials, as well as biological tissues, exhibit viscoelasticity to varying degrees.

Noncrystalline or semicrystalline polymers and glasses exhibit free volume and a *glass transition temperature* (T_g) due to the inability of relatively large molecules to organize into a perfectly crystalline network. Below T_g, molecular motions are restricted by time, and the material exhibits glassy or brittle elastic behavior. Near T_g, or more precisely within a temperature range surrounding T_g, the free volume allows some viscous molecular rearrangement and the material exhibits a viscoelastic response, which becomes increasingly elastomeric (nonlinear elastic) with increased temperature above T_g. Near the melting temperature, elastic deformation is lost and the material exhibits only viscous flow. Additional background on structure-property relationships – including the effects of molecular weight, crystallinity, cross-linking, etc. – for noncrystalline and semicrystalline materials (polymers and glasses) is available in a number of textbooks [5–8,96]. Hydrated biological tissues can also exhibit viscoelasticity due to the permeability of the tissue to fluid flow (poroelasticity).

Constitutive models for creep and stress relaxation in viscoelastic materials utilize numerous combinations of two simple elements used as mechanical analogs (Fig. 3.9). A spring element models time-independent elastic behavior, as described in Section 3.2. A dashpot element models time-dependent viscous behavior as $\dot{\varepsilon} = \sigma/\eta$, where $\dot{\varepsilon}$ is the strain rate (normal or shear), σ is the applied stress (normal or shear), and η is the viscosity. In polymers, elastic behavior is due to strong covalent intramolecular bonds, while viscous behavior is due to weak intermolecular van der Waals bonds. Thus, the viscoelastic behavior of thermoplastic polymers lies somewhere in-between these two extremes.

The classic *Maxwell model* combines a spring and dashpot in series to model viscoelastic stress relaxation, but the prediction of Newtonian flow

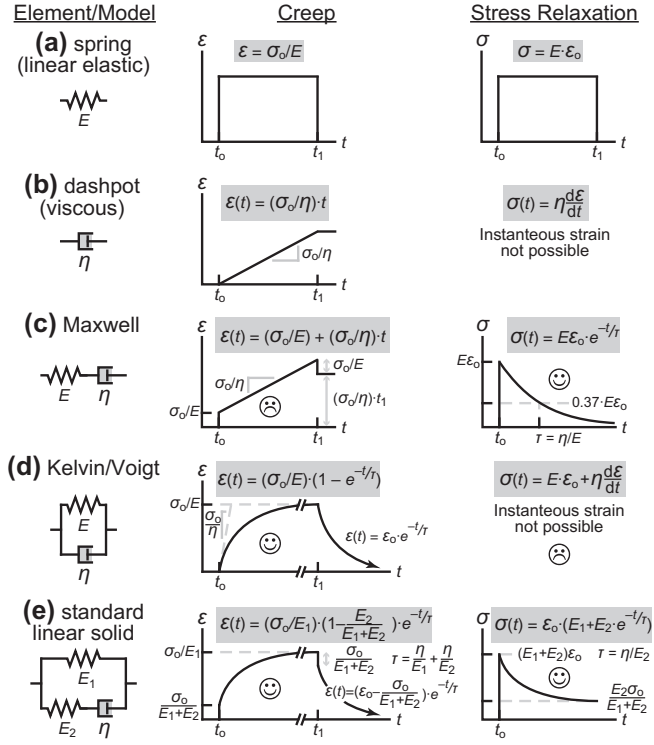

FIGURE 3.9 Common viscoelastic constitutive models for viscoelastic creep and stress relaxation, due to an instantaneous and constant applied stress (σ_o) and strain (ε_o), respectively, including (a) a spring element, (b) a dashpot element, (c) the Maxwell model, (d) the Kelvin or Voigt model, and (e) the standard linear solid model, where t is time, E is the elastic modulus of spring elements, η is the viscosity of dashpot elements, and τ is the relaxation time.

during creep or strain recovery is not realistic, and stress relaxation does not necessarily decay to zero (Fig. 3.9c). Conversely, the classic *Kelvin* or *Voigt model* combines a spring and dashpot in parallel to model viscoelastic creep, but stress relaxation is not possible and creep deformation may be erroneous at short times (Fig. 3.9d). By combining the strengths of the Maxwell and Kelvin models, the *standard linear solid model* (a.k.a., the three-parameter model) provides a good approximation of both creep and stress relaxation for the most linear viscoelastic polymers (Fig. 3.9e), although the stress relaxation may be more rapid than reality as has been shown for bone tissue [97]. In each of the above models, creep and stress relaxation are most accurately modeled by an exponential rise and decay, respectively, characterized by a time constant or *relaxation time* (τ), which is a function of spring stiffness and dashpot viscosity. The *Burgers model* (a.k.a., four-parameter model) also combines the Maxell and Voigt models in series and is popular. The *generalized Maxwell*

model combines a spring in parallel with n Maxwell elements, and the *generalized Kelvin model* combines a series of n Kelvin elements such that $n = 4$ to 6 is sufficient to fit the stress relaxation and creep of nearly any data. However, models with more than several parameters become physically less meaningful, beyond experimental capabilities, and increasingly difficult to calculate.

Reliable creep (see also Section 3.4.3.2) and stress-relaxation [98,99] characterization requires particularly well-defined specimens (see Section 3.3), precise instrumentation (see Section 3.4.1) suitable for small deformations and low rates, and precise control or monitoring of temperature and humidity (see Section 3.5). Specimens are typically preconditioned at the highest temperature to be analyzed by applying the maximum load for the maximum time period, followed by unloading to allow recovery over a period 10 times longer than the loading period, and repeating this procedure until achieving reproducible behavior. Preconditioning promotes fully recoverable deformation and erases memory of prior thermomechanical history. Due to the likelihood of relatively large strains in viscoelastic materials, load levels should be chosen or altered such that the specimen cross-section remains under constant stress. Step loads and deformations are typically applied in uniaxial tension, uniaxial compression, bending, or torsion [98]. Compression can be problematic due to buckling or barreling, and bending can be problematic due to nonuniform stress/strain. However, bending can be advantageous for load fixtures, applying small loads, and measuring small strains by amplified deflections. In torsion, shear stress and strain can be substituted in Fig. 3.9 in place of normal stress and strain [97]. A strain rate that is too high may result in damped vibrations in a creep experiment, while a low strain rate may result in a low, noninstantaneous stress for stress relaxation. Acceptable deviation from the assumption of an initial instantaneous stress or strain should be compensated by shifting t_o (Fig. 3.9) to the point where the maximum strain or stress, respectively, is achieved in a creep or stress relaxation test [98,99]. Finally, creep tests should be performed over a sufficient time scale to examine the possibility of accelerated creep at long times or nonlinear viscoelasticity requiring corresponding constitutive equations [96].

A full understanding of viscoelastic behavior requires testing over a wide range of time (or frequency) and temperature. Fortunately, time–temperature equivalence may be used to measure, for example, creep or relaxation data over a short time period at several temperatures, enabling the effective response to be known over several orders of magnitude of time [5,96]. Experimental characterization may not only utilize transient measurements of creep and stress relaxation, as described above, but also cyclic loading, which will be discussed in the following section. Creep and stress-relaxation tests are conducted at low frequency (<1 Hz), while higher frequency analysis may employ free or forced oscillations (10^{-2} to 10^{2} Hz, e.g., DMA), resonant vibrations (10^{2} to 10^{4} Hz), and wave propagation ($>10^{4}$ Hz).

3.4.4. Frequency and Time-Dependent Behavior

The frequency of loading, or cyclic loading, is another aspect of time-dependent behavior which is also critical for mechanical characterization of biomaterials. Biomaterials and biomedical devices are typically subjected to cyclic mechanical loading in service due to repetitive voluntary activities, such as running or walking, and involuntary muscle contractions, such as in the cardiovascular system. Cyclic loading can lead to fatigue deformation and fracture, as well as creep and stress relaxation in viscoelastic materials.

3.4.4.1. Cyclic Loading and Fatigue

Cyclic mechanical loading can lead to *fatigue* failure at significantly lower stress levels than would be expected to cause failure under quasistatic loading. Fatigue can be divided into a three-stage process including (I) *crack initiation* at local stress concentrations due to defects and microstructural inhomogeneities (e.g., inclusions, grain boundaries, pores, surfaces, etc.), (II) *crack growth* when a stage I crack reaches a critical size, and (III) *fatigue fracture* when the remaining uncracked cross-sectional area is unable to sustain the maximum applied tensile stress in a loading cycle. Predictive methods for fatigue failure primarily consider stage II crack growth rates, as described below. Examination of fatigue failure surfaces reveals *beachmarks* that are visible to the naked eye and show intermittent bursts of crack growth due to discontinuous loading, and *striations*, which are visible with an electron microscope and show increments of crack growth for each loading cycle during stage II (Fig. 3.10).

Fatigue tests specify a waveform, frequency, cyclic stress (stress-controlled) or strain (strain-controlled) levels, loading mode, and test duration. Sinusoidal waveforms (Fig. 3.11a) are most commonly employed due to the relative ease of controlling gradual changes in stress/strain. However, a square or triangular waveform may be employed when impulse loading or a constant strain rate, respectively, is necessary, but can pose greater difficulty with control. In all cases, additional precautions must be taken to properly calibrate load cells for cyclic loading [100]. Moreover, most test instruments utilize proportional-integral-derivative control systems that must be properly tuned for the desired waveform and frequency [101]. The loading frequency may range from 10^{-2} to 10^{2} Hz, but is most commonly of the order of 1 Hz for biomaterials and biomedical devices as this frequency is similar to that of walking or a beating heart. Greater frequencies may be employed for accelerated tests or simulating higher levels of activity, but a greater loading frequency for a fixed stress imposes a greater strain rate. Therefore, the fatigue behavior of the strain rate-sensitive materials (e.g., viscoelastic materials) will be highly sensitive to the loading frequency. Moreover, a loading frequency above 5 Hz can result in the heating and melting of thermoplastic polymers. On the other hand, loading frequency can be leveraged to measure viscoelastic material properties, as discussed further in Section 3.4.4.4.

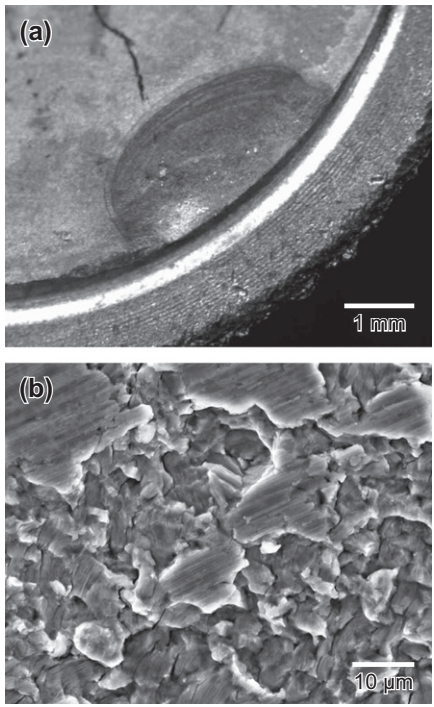

FIGURE 3.10 (a) An optical micrograph showing beachmarks and (b) an SEM micrograph showing striations on the failure surface of a Ti-6Al-4V hip stem retrieved after fracturing 26 months into service.

Cyclic stress (or strain) levels are characterized by the *maximum stress* (σ_{max}), *minimum stress* (σ_{min}), *stress amplitude* (σ_a), *mean stress* ($\overline{\sigma} = (\sigma_{max} + \sigma_{min})/2$), *stress ratio* ($R = \sigma_{min}/\sigma_{max}$), and *stress range* ($\Delta\sigma = \sigma_{max} - \sigma_{min} = 2 \cdot \sigma_a$) (Fig. 3.11a). In *fully reversed fatigue*, the stress amplitude oscillates between tensile and compressive stresses equal in magnitude and the mean stress is zero ($R = -1$), while *tension–tension fatigue* has a mean stress greater than zero ($0 < R < 1$). Fatigue tests commonly utilize $R = 0.1$ such that that specimen is never fully unloaded in order to avoid slack in loading fixtures, but yet $\sigma_a \approx \sigma_{max}$ [102]. Fatigue testing of materials normally utilizes fixed stress (stress-controlled) or strain (strain-controlled) levels, e.g., a constant stress amplitude and waveform [102–107]. The effects of variable loading amplitude and/or irregular loading history can be approximated by Miner's rule [5,7], which may be useful for failure analysis but is not recommended for biomaterials characterization. Thus, constant-amplitude fatigue is most useful for biomaterials characterization, and the following discussion will consider stress-controlled fatigue, although strain-controlled fatigue is also used and discussed in detail elsewhere [7,108].

The simplest and most common fatigue tests utilize specimens with uniform cross-section loaded axially (Fig. 3.7), either in tension–tension or fully

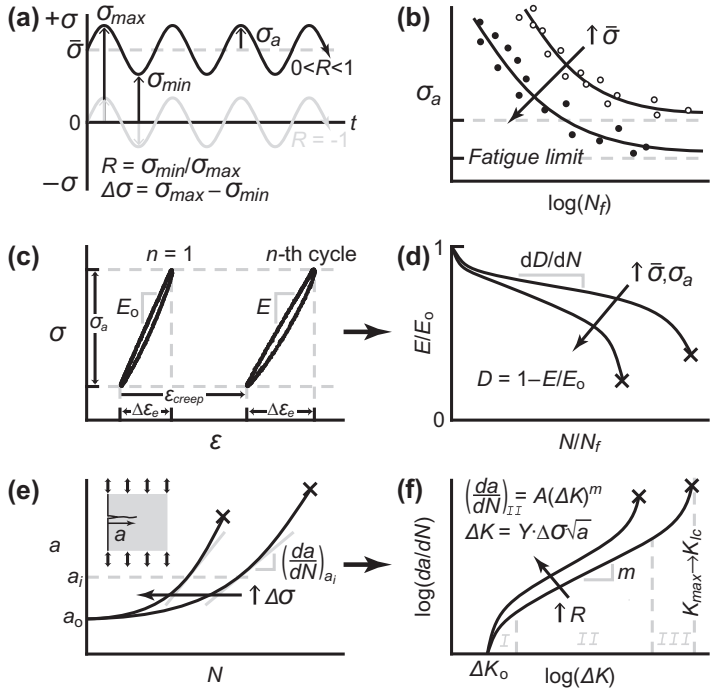

FIGURE 3.11 (a) Schematic diagram showing sinusoidal cyclic stresses applied in stress-controlled fatigue tests where σ_a is the stress amplitude, σ_{max} is the maximum applied stress, σ_{min} is the minimum applied stress, $\overline{\sigma}$ is the mean applied stress, R is the stress ratio, and $\Delta\sigma$ is the stress range. (b) "*S-N* curves" showing the fatigue life (N_f) and fatigue limit for a material after conducting numerous fatigue tests at varying, controlled levels of stress amplitude (σ_a). (c,d) Degradation, or damage (D), and creep deformation (ε_{creep}) during a fatigue test may be measured by changes in the secant or tangent modulus (E) and translation of cyclic stress–strain hysteresis loops during a test, where $\Delta\varepsilon_e$ is the recoverable elastic strain for each loading cycle. (e,f) Fatigue crack propagation tests measure the stage II crack growth rate (da/dN) from a pre-existing notch or crack (a_o) for a stress-intensity factor range (ΔK), where A and m are empirical constants, and Y is geometric factor for the specimen (see Section 3.2.6).

reversed tension–compression [102–107]. Flexural fatigue testing most commonly utilizes a rotating beam [109] and cyclic four- or three-point bending [110]. Rotating beam tests can be useful as a lower cost option for material screening. Flexural fatigue tests may also be used for the same reasons described above for quasistatic loading, but are also subject to the same potential complications and limitations (see Section 3.4.2). Thus, flexural fatigue may [111] or may not [112] provide a suitable option and should be used judiciously. Biaxial loading [113,114] and torsion [115] may also be useful for specific devices but are less common for biomaterials characterization.

3.4.4.2. Fatigue Life and Damage

Fatigue lifetime test data are most commonly reported as an *S-N curve*, which plots the stress amplitude (σ_a) versus the *number of cycles to failure* (N_f) for a number of test specimens on log–log or semi-log axes (Fig. 3.11b). The *fatigue life* is the number of cycles to failure at a given stress level. The *fatigue strength* is the stress corresponding to a given number of cycles to failure. The *fatigue limit* is the stress level at which the fatigue failure will never (at least practically speaking) occur. Thus, an increased stress level results in a decreased fatigue life. Increasing the mean stress results in a shorter fatigue life for a given stress amplitude and a lower fatigue limit. Specimens that survive a designated number of cycles without failure (often 10^7 or 10^8) are designated as a run-out, which often serves as a default fatigue limit, but run-out data points must be excluded from statistical or empirical analyses of *S-N* curves. *S-N* curves are commonly fit empirically using a power-law (Basquin equation) as $\sigma_a = \sigma_f \cdot N_f^b$, where σ_f is the fatigue strength coefficient which is comparable to the quasistatic fracture strength and b is the Basquin exponent, or using other empirical models [116]. Moreover, a number of empirical models (e.g., Goodman, Gerber, Soderberg) can be used to relate the fatigue limit to the stress amplitude and mean stress [5–8]. Statistical analysis of fatigue life and fatigue strength data typically requires the use of a logarithmic distribution or nonparametric tests [103,116]. Since fatigue behavior is inherently variable and sensitive to defects, confidence intervals are often reported for *S-N* data [103,105,116]. Furthermore, a Weibull analysis for the probability of failure is often very useful for characterizing fatigue life and fatigue strength data [107,116,117], including data sets with run-out specimens, similar to methods used for quasistatic fracture strength (Section 3.2.6).

The presence of a stress concentration can significantly decrease the fatigue life of a material, similar to the effects previously described for strength and fracture toughness (Section 3.2.6). Therefore, the above methods may also be applied to testing notched specimens. The behavior of notched versus un-notched specimens is characterized by a *fatigue notch factor*, $k_f = \sigma_a / \sigma_{a,notched}$, where σ_a and $\sigma_{a,notched}$ are the stress amplitudes or fatigue strengths for the un-notched and notched specimens, respectively, at the same number of loading cycles. Metals and polymers that are otherwise ductile can exhibit a shorter fatigue life and more brittle behavior in the presence of a notch or stress concentration [109,118,119].

Mechanical properties are degraded during the course of a fatigue test, as evidenced from changes in the stress–strain hysteresis loops (Fig. 3.11c). The secant or tangent modulus (E) may decrease due to various *damage* processes, including microcracking in quasi-brittle materials (e.g., bone [112,120,121] and acrylic bone cement [117]), or cyclic softening and void formation (including crazing) in ductile materials. Note that while most metals and alloys exhibit cyclic softening, some ductile metals can exhibit cyclic hardening. Moreover, crazing can also lead to an increased modulus early in the fatigue life

of thermoplastics due to orientation strengthening [111]. A damage parameter can be defined as $D = 1 - E/E_o$, where is E_o is the initial secant or tangent modulus, such that the amount and rate (dD/dN) of damage accumulation can be measured during a test as a function of the number of cycles or fatigue life (Fig. 3.11d) [120,121]. In stress-controlled fatigue, the entire hysteresis loop may also translate to higher strains indicative of a permanent *creep strain* (ε_{creep}) (Fig. 3.11c), which may also be measured as a function of the number of cycles [111,112,121–123]. Finally, *strain energy dissipation* can be measured by the area of the hysteresis of each loading cycle (Fig. 3.11c), due to processes such as microcracking, plasticity, adiabatic heating, etc., and may also be measured as a function of the number of cycles [111,120].

3.4.4.3. Fatigue Crack Propagation

Fatigue crack propagation integrates fracture mechanics concepts with fatigue in order to characterize the stage II crack growth rate. Standardized specimens (e.g., compact tension) are precracked (see Section 3.3.2), and crack growth (da) is measured as a function of loading cycles (N) using a traveling microscope, specimen compliance, and/or electrical resistance [23,124]. The crack growth rate increases throughout the fatigue lifetime until failure, and increased stress levels increase the crack growth rate at a given number of cycles (Fig. 3.11e). Fracture mechanics is integrated by calculating a stress intensity factor range ($\Delta K = K_{max} - K_{min}$) from the stress range (see Section 3.2.6). The stress intensity factor range is related to the *crack growth rate* by the *Paris Law*, $da/dN = A \cdot \Delta K^m$, where A and m are empirical constants dependent on the material properties, environment, loading frequency, and stress ratio [23]. The exponent is usually in the range of $2 < m < 10$. A log–log plot of da/dN versus ΔK reveals the three stages of fatigue described above (Fig. 3.11f), initiated by a threshold stress intensity range (ΔK_o) for fatigue crack propagation and ending with fracture as K_{max} approaches K_{Ic}, although typically only stage II is plotted. An increased stress ratio results in increased da/dN (or m) and decreased fatigue life. Once the empirical constants of the Paris Law are known, the fatigue life can be predicted by integrating the Paris Law from an initial to final crack length [5–8,23]. Moreover, the striation spacing (s) measured from electron micrographs of failure specimens or retrievals can be used to estimate or confirm ΔK as $s = A_s \cdot (\Delta K/E)^2$, where A_s is the Bates–Clark constant, which is a material-dependent empirical constant [125,126]. Finally, the stress intensity range in fatigue crack propagation tests can be modified to account for plasticity using plastic-zone size correction factors or the J-integral [23], similar to fracture toughness measurements, and the Paris Law can also be modified to account for combined creep [127].

3.4.4.4. Dynamic Mechanical Analysis

Cyclic loading of a viscoelastic material will result in a time delay or phase shift between the applied stress and strain response. DMA utilizes this behavior to

characterize the viscoelastic properties of materials, typically polymers [5,96,128]. A sinusoidal stress takes the form, $\sigma(t) = \sigma_o \cdot \sin(\omega t + \delta)$, where t is time, ω is the angular frequency ($\omega = 2\pi f$) in rad/s, f is the ordinary frequency in Hz, and δ is the *phase angle* of the time delay for the lagging strain response, $\varepsilon(t) = \varepsilon_o \cdot \sin(\omega t)$. The stress can be expanded into an elastic in-phase component reflecting strain energy stored and released, $\sigma_o \cdot \cos(\delta)$, and a viscous out-of-phase component reflecting dissipated strain energy, $\sigma_o \cdot \sin(\delta)$. Therefore, the *storage modulus* is measured as $E' = (\sigma_o/\varepsilon_o) \cdot \cos(\delta)$; the *loss modulus* is measured as $E'' = (\sigma_o/\varepsilon_o) \cdot \sin(\delta)$; and $E'/E'' = \tan(\delta)$. The storage and loss moduli can also be determined as shear moduli (G', G''). Storage and loss moduli for polymers can vary dramatically with changes in the loading frequency and temperature, enabling determination of the glass transition temperature (as well as other secondary transitions) and relaxation times, respectively. DMA is advantageous over creep and stress relaxation tests in obviating the need for long time periods to measure time constants.

Similar to creep and stress relaxation tests (Section 3.4.3), DMA requires well-defined specimens, precise instrumentation, precise control or monitoring of temperature and humidity, and possibly preconditioning [129]. DMA instruments employ either free oscillation, most commonly using a torsion pendulum, or forced oscillation in a variety of possible loading modes (uniaxial tension, compression, torsion, bending, and in-plane shear). The torsion pendulum is a simple test but limited by decreasing stress/strain amplitude with time and a dependence of frequency on the material properties. Forced oscillation tests are more complex but also more reproducible and able to investigate a wider frequency and temperature range.

3.4.5. Nondestructive Tests

Almost all of the preceding tests discussed in this chapter are considered *destructive tests*, as the specimen is loaded until failure occurs by permanent deformation or fracture. While single cycle elastic deformation of a specimen or DMA could be considered nondestructive, *nondestructive testing* is usually used to describe tests that can be performed on a material or device prior to or during service without any detrimental affect on performance. Nondestructive tests for mechanical characterization of biomaterials primarily include indentation and ultrasound, and these will be introduced below. Other methods of nondestructive evaluation are primarily used to detect flaws or aspects of material structure associated with, and likely causal for, changes in mechanical properties. Broadly categorized, these methods utilize X-rays (e.g., radiography, computed tomography), electromagnetics (e.g., magnetic resonance imaging, magnetic flux leakage, magnetic particle testing, eddy current testing), sound and vibration (e.g., ultrasound, acoustic emission, resonance), visible and infra-red light (e.g., penetrants, interferometry, thermography) to detect flaws or changes in microstructure [130].

3.4.5.1. Indentation

Indentation methods utilize an indenter of specified geometry (Table 3.1) that upon loading and elastic unloading leaves a permanent indentation in the specimen. Thus, indentation tests could be excluded from a strict definition of nondestructive testing due to localized permanent deformation providing a stress concentration that could lead to failure. If used prior to service, indentations must be verified to not compromise the biomaterial or device performance, e.g., by placement in locations experiencing little or no stress in service. Thus, indentation tests have been historically utilized for quality control, but their utility for biomaterials characterization is primarily found in sampling small volumes of material and/or characterizing gradients or heterogeneity in mechanical properties. Moreover, many methods for specimen preparation prior to indentation tests are also necessarily destructive.

Indentation tests measure the *hardness* (H) of a material, which is the resistance to permanent deformation by the indenter and can thus be correlated with the yield strength (e.g., $H \approx 3 \cdot \sigma_y$ for many metals), elastic modulus, and other mechanical properties [131]. A number of different indenters, corresponding hardness scales, and common applications are summarized in Table 3.1. Spherical indenters (Hertzian contact) and spheroconical diamond indenters are used with relatively high applied loads for traditional *Brinell and Rockwell hardness* tests for bulk material properties [132–134]. Brinell tests measure the "true hardness" as the ratio of applied load to the projected contact area (A_c) of the indentation, but produce large indentations requiring large loads. Rockwell tests have enjoyed decades of commercial popularity due to providing rapid, reliable results, a small indentation area, and a wide range of scales (A, B, C, D, etc.) suitable for almost all materials. However, Rockwell hardness is measured as a nondimensional number corresponding to the difference in the depth of indenter penetration between an applied load and a preload, after a specified hold time, and must be empirically converted to true hardness [135].

Microhardness tests are particularly useful for sampling a small volume of material (e.g., films, coatings, and microstructural features) and/or characterizing gradients or heterogeneity in mechanical properties at the microscale. *Knoop and Vickers hardness* utilize sharp diamond pyramid indenters (Table 3.1) that require much lower loads and leave indentations requiring an optical microscope for measuring the indentation size [136–138]. Knoop and Vickers can also be used at higher loads to characterize bulk material hardness and to characterize anisotropy via differences in indentation diagonal lengths relative to the specimen orientation. Knoop indenters are well suited for measuring hardness in brittle materials due to producing a small indentation depth. Conversion tables are available for relating Brinell, Rockwell, Knoop, and Vickers hardness, but are material-specific [135]. Brinell, Knoop, and

TABLE 3.1 Common Indenters, Hardness Scales, and Applications for the Mechanical Characterization of Materials by Indentation and Instrumented Indentation

Indenter Type/Hardness Scale			α	P	Indent	H	A_c	Common Applications
Sphere (Hertzian)	WC or steel D = 1, 2.5, 5, 10 mm (Brinell)		n/a	1–3000 kgf		$BHN = \frac{2P}{\pi d \cdot (D - \sqrt{D^2 - d^2})}$	$\pi(D \cdot h_c - h_c^2)$	Ductile metals polymers
	WC or steel D = 1/16,1/8, 1/4, 1/2 in (Rockwell B,E,F,G,K,L,M,R)		n/a	60–150 kgf		$HRX = 130 - (h_c/0.002)$	$\pi(D \cdot h_c - h_c^2)$	Ductile metals polymers
Spheroconical diamond (Rockwell A,C,D)			60°	60–150 kgf		$HRX = 100 - (h_c/0.002)$	$\pi h_c^2 \cdot \tan^2(\alpha)$	Hard metals ceramics
Diamond pyramids	Knoop		α_1 = 86.25° α_2 = 65°	1–120 kgf (macro) 1–1000 gf (micro)		$KHN = \frac{2P}{d_1^2 \cdot \cot(\alpha_1) \cdot \tan(\alpha_2)}$	$2h_c^2 \cdot \tan(\alpha_1) \cdot \tan(\alpha_2)$	Hard metals ceramics microhardness

(*Continued*)

TABLE 3.1 Common Indenters, Hardness Scales, and Applications for the Mechanical Characterization of Materials by Indentation and Instrumented Indentation—cont'd

Indenter Type/Hardness Scale		α	P	Indent	H	A_c	Common Applications
	Vickers 	68°	1–120 kgf (macro) 1–1000 gf (micro) ~10 nN – 10 N (nano)		$VHN = (2P/d^2)\cdot\sin(a)$ $H_{nano} = P/A_c$	$4h_c^2\cdot\tan^2(\alpha)$	Hard metals ceramics microhardness toughness nanoindentation
	Berkovich 	65.3°	~10 nN – 10 N		$H_{nano} = P/A_c$	$3\sqrt{3}\cdot h_c^2\cdot\tan^2(\alpha)$	Nanoindentation
	Cube corner 	35.3°	~10 nN – 10 N		$H_{nano} = P/A_c$	$3\sqrt{3}\cdot h_c^2\cdot\tan^2(\alpha)$	Nanoindentation toughness
Circular flat punch hardened steel D = 0.25–1.5 mm		90°	~10 nN – 10 N		$H_{nano} = P/A_c$	$\pi d^2/4$	Viscoelastic and/or highly compliant materials

D is the indenter diameter, α is the angle between the vertical centerline and contact face(s) of the indenter, P is the applied load, d_1 and d_2 are orthogonal measurements of the indentation diameter or diagonal, d is the mean indentation diameter or diagonal, H is hardness, BHN is the Brinell hardness number, HRX is the Rockwell hardness number for any scale (X = A, B, C, D, etc.), KHN is the Knoop hardness number, VHN is the Vickers hardness number, H_{nano} is the hardness measured by nanoindentation, A_c is the projected contact area of the indentation, and h_c is the indentation depth.

Vickers hardness are typically reported in MPa by multiplying units of kgf/mm^2 by 9.807 m/s^2.

There has been a resurgence of interest in indentation tests over the last 20 years due to the development of *instrumented indentation* and *nanoindentation* [139–141]. Rather than simply applying a fixed load, instrumented indentation enables load and displacement measurement throughout loading and elastic unloading of the indenter. Therefore, a *reduced modulus* (E_r) for the specimen and indenter materials can be measured as $(S/2\beta)\cdot(\pi/A_c)^{1/2}$, where S is the unloading stiffness measured by taking the derivative of a nonlinear least-squares power-law fit to the unloading curve at P_{max}, β is a nondimensional parameter used to account for any deviations from the ideal solution (e.g., $\beta \approx 1.034$ for a Berkovich indenter), and A_c is the projected contact area of the indention [139]. The contact area is calculated from the ideal indenter geometry as a function of the contact depth (h_c), using the equations in Table 3.1 [140]. The contact depth is calculated as $h_c = h_{max} - (\varepsilon \cdot P_{max})/S$, where h_{max} is the indenter depth at P_{max} and ε is a geometric constant ($\varepsilon \approx 0.75$ for most indenters) [139]. Note that the equations for A_c in Table 3.1 are ideal and are calibrated in practice to account for the indenter tip rounding and other deviations [139]. The *indentation modulus* (E_i) of the specimen can be determined from the reduced modulus using the relation, $1/E_r = (1-\nu^2)/E_i + (1-\nu_I^2)/E_I$, where ν is Poisson's ratio of the specimen material, and ν_I and E_I are the Poisson's ratio and elastic modulus of the indenter material. For diamond, $\nu_I = 0.07$ and $E_I = 1141$ GPa. If Poisson's ratio is not known for the specimen material, the plane strain indentation modulus can be reported as $E_i' = (1-\nu^2)/E_i$.

The use of sharp diamond indenters (Berkovich, cube corner, and Vickers) combined with precise instrumentation and control (via electrostatic or electromagnetic actuation and capacitive or inductive transducers) enables nanoscale resolution within the range of both the applied load (~10 nN – 10 N) and indentation depth (~1 nm – 20 μm), hence the term "nanoindentation." *Nanoindentation hardness* (H_{nano}) is thus measured as P_{max}/A_c (Table 3.1). The three-sided Berkovich and cube-corner indenters are more readily machined to a sharp tip compared to Vickers and Knoop indenters, making them best suited for instrumented nanoindentation, as well as imaging and mechanical characterization using atomic force microscopy.

In all indentation tests, the indenter material must have greater hardness than the specimen material. An appropriate load must be selected based on the specimen material, indenter type, and hardness scale (Table 3.1). The size of the indentation (depth) can influence the measured hardness or modulus and should thus be controlled and documented for comparison of results, regardless of whether the size effect is artifactual or real. The applied load is also always held for a specified period of time to remove or control effects of strain-rate sensitivity or creep. Other important requirements include flat specimen surfaces, surface roughness less than 10% of the indentation depth, a specimen

thickness at least 10-times the indentation depth, spacing between the center of indentations and the specimen edge of at least 2.5 indentation diameters, and spacing between the center of indentations of at least 3 indentation diameters, although the recommended indentation spacing varies slightly between standards [132,133,136–138].

Indentation can also be used to characterize viscoelastic and compliant biomaterials. *Durometer hardness* is used to characterize the bulk hardness of viscoelastic and elastomeric polymers [142]. *Creep* and *stress relaxation* time constants can be measured by varying holding times (typically 3–120 s), loading and unloading rates, or by fitting data to viscoelastic models (see Section 3.4.3.3) [97,141]. *Dynamic nanoindentation* may also be used to measure the storage and loss moduli [140]. A spherical or *circular flat punch indenter* (Table 3.1) may be useful for characterizing viscoelastic and highly compliant biomaterials [143,144]. Note that fluid cells are also available to maintain specimens in a hydrated environment.

Indentation testing has also been used to measure *indentation fracture toughness* in relatively brittle materials. A sufficiently high load applied to a Vickers indenter in a brittle material was observed to result in cracks propagating away from indentation edges at and below the surface as "half-penny" cracks. Numerous solutions have been proposed and used for Vickers indentation fracture toughness ($K_{c,i}$) but the most common is $K_{c,i} = 0.16 \cdot P \cdot (E/H)^{1/2} \cdot (c_o)^{-3/2}$, where P is the applied load, E/H is the elastic modulus to hardness ratio, and c_o is the radius of the half penny crack measured at the specimen surface from the center of the indent to the crack tip [145,146]. The E/H ratio can be experimentally measured on the same specimen using Knoop indentations as $E/H = 0.45/(0.14 - d_2/d_1)$, where d_2 and d_1 are the short and long diagonals, respectively, of the indentation [147]. The lower centerline-face angle (α) of a cube corner indenter relative to a Vickers indenter results in crack formation at lower loads and thus smaller indentations. Therefore, cube corner indenters have also been used for measuring indentation fracture toughness with similar equations [145]. However, indentation fracture toughness measurements are not equivalent to plane strain fracture toughness (K_{Ic}), are subject to large errors, and are difficult to perform in a hydrated environment [145]. Therefore, indentation fracture toughness should be used cautiously and only compared between tests using identical methods and similar materials. Nonetheless, indentation fracture toughness can occasionally be useful for materials and situations where plane strain fracture toughness measurements are not possible due to the available specimen size, or for characterizing heterogeneity over small distances, provided that results are treated as semiquantitative.

In summary, indentation testing enables the mechanical characterization of biomaterials at spatial scales not possible by other methods. However, there are also a number of inherent limitations for indentation testing. (1) Hardness is an aggregate property reflecting the effects of a number of material properties.

(2) Indentation tests tend to produce semiquantitative results due to the need for approximations and correction factors to describe the true indentation shape. (3) Indentations tests are highly sensitive to the indenter geometry and test parameters. Therefore, instrument calibration is critical using test blocks for hardness and microhardness, and using detailed procedures for instrumented nanoindentation that are described elsewhere [139,140]. Finally, material properties (e.g., E_i) measured by indentation should not be treated as equivalent nor directly compared between different indentation methods or with other test methods.

3.4.5.2. Ultrasound

Ultrasound is primarily thought of as an imaging technique, but ultrasonic wave propagation can also be used to measure the elastic constants, or stiffness coefficients, of a material nondestructively and precisely [148]. Thus, elastic anisotropy can be characterized on a single specimen [149,150], whereas destructive tests require multiple tests (e.g., uniaxial tension and torsion) on multiple specimens to fully characterize anisotropy. The high frequency of ultrasound ensures purely elastic deformation, even in viscoelastic materials. Ultrasound can also be used with small specimens (mm-scale) [151], enabling the characterization of gradients or heterogeneity in the magnitude and anisotropy of elastic constants at the mesoscale [152]. Moreover, scanning acoustic microscopy can be used to generate acoustic images with up to 1 μm spatial resolution on thin, planar specimens [153]. Finally, ultrasound is well-suited for testing biomaterials and tissues in a hydrated environment.

Ultrasonic waves are generated and received by piezoelectric transducers operating in the kHz–MHz range. The transducer frequency should be chosen considering the specimen size and material properties. The minimum specimen distance that can be resolved is $n \cdot \lambda/2$, where n is the number of wavelengths, λ is the wavelength ($\lambda = v/f$), v is the wave velocity, and f is the frequency [154]. Waves may be continuous [150], or pulsed [149,151,152] to generate an intense burst to aid detection. The pulse width is the most critical parameter governing the minimum specimen distance that can be resolved [154]. The "through-transmission" method uses two transducers to separately transmit and receive the wave on opposite sides of the specimen (Fig. 3.12a). The reflection ("pulse-echo") method uses a single transducer to transmit and receive a wave after reflecting on the opposite specimen surface. Transducers can generate either normal (a.k.a., longitudinal) or shear (a.k.a., transverse) waves (Fig. 3.12b). Signal transmission from the transducer to the specimen is aided by using a liquid couplant. Water generally suffices for normal waves, which is advantageous, if not necessary, for biomaterials characterization. However, shear waves typically require a high-viscosity couplant, such as honey, glycerin, or propriety products, which are water soluble and are readily removed from the specimen surface after testing.

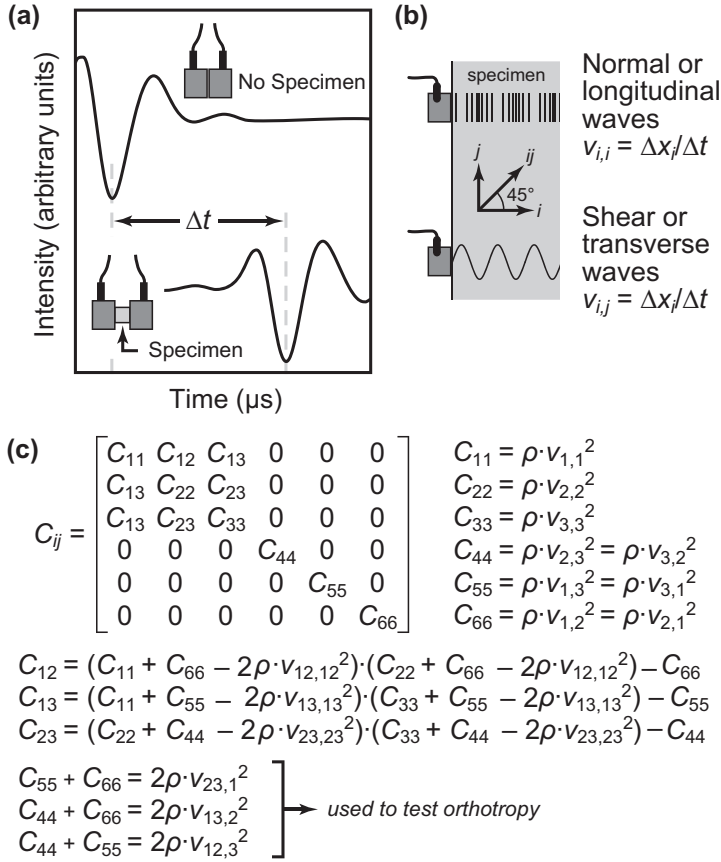

FIGURE 3.12 Characterization of anisotropic elastic constants using the pulse transmission method for ultrasonic wave propagation between two transducers: (a) Schematic diagram showing the time delay (Δt) for transmission of an ultrasonic wave pulse through a specimen as measured on an oscilloscope. (b) Schematic diagram showing the propagation of normal (or longitudinal) and shear (or transverse) waves in a specimen by corresponding ultrasonic transducers and the calculation of the wave velocity (v), where Δx is the specimen distance traversed by the wave. Note that the directions of wave propagation and displacement are coincident for normal waves but orthogonal for shear waves ($v_{i,j}$), where i is the direction of wave propagation and j is the direction of displacement. (c) Equations used to measure all elastic constants (C_{ij}) in an orthotropic material and to test the condition of orthotropy, where ρ is the apparent density of the specimen material, $v_{ij,ij}$ is the velocity for wave propagation in the ij direction and displacement in the ij plane, and $v_{ij,k}$ is the velocity for wave propagation in the ij direction and displacement in the k direction.

The use of normal and shear waves propagating in various specimen directions can be used to directly measure all the *elastic constants* of an orthotropic material (see Section 3.2.5) using the equations in Fig. 3.12c. The wave velocity (v) for a normal or shear wave is measured by the time delay (Δt)

for wave transmission through the specimen (Fig. 3.12a) in a particular direction over a distance, Δx (Fig. 3.12b). The distance traversed by the wave is usually measured by digital calipers, and the time delay is measured using an oscilloscope connected to the transducers and wave signal generator. The general solution for elastic wave propagation in a one-dimensional solid is $C = \rho \cdot v^2$, where C is the elastic constant or stiffness coefficient, ρ is the apparent density of the specimen material, and v is velocity of a normal or shear wave in the appropriate specimen direction and orientation (Fig. 3.12c). The apparent density of the specimen is typically measured by Archimedes principle using standardized methods [155,156]. Engineering constants (elastic moduli, shear moduli, and Poisson's ratios) can be extracted from the compliance tensor (S) after inverting the measured elastic constant tensor [6,149,150].

The advantage of nondestructive characterization is also the cause of the main limitation of ultrasound, which is that only elastic constants (or moduli) can be measured. Moreover, while ultrasound is nondestructive for the specimen, measurements of elastic heterogeneity and anisotropy typically require destructive sectioning of the device or a larger sample. Parallel specimen surfaces are required for both the through transmission and reflection techniques. The most fundamental and common methods for ultrasonic mechanical characterization of material were described above, but many other methods are available for mechanical characterization, including oblique through transmission, ultrasonic wave attenuation, ultrasonic resonance spectroscopy, Rayleigh and Lamb surface waves, etc. [148], as well as the closely related technique of acoustic emission.

3.5. ENVIRONMENT

Tabulated mechanical properties of engineering materials are typically characterized in air at ambient temperature and pressure. However, biomaterials are typically subjected to various sterilization methods prior to service and an aqueous physiological environment in service. Therefore, mechanical characterization of biomaterials often warrants the consideration of temperature, pressure, aqueous media containing various chemicals, and irradiation, which may each lead to degradation of mechanical properties.

3.5.1. Temperature and Pressure

Deviation from ambient temperature and pressure may occur due to any of three common extremes. Implantable biomaterials function at body temperature (37 °C) in service. Steam sterilization occurs in an autoclave at temperatures and pressures up to 134 °C and 207 kPa, respectively. Biomedical materials that may be subjected to steam sterilization includes not only the materials used in implantable devices and surgical instruments but also the

materials used in cases, trays, and packaging for the implantable devices and instruments. Finally, cryopreservation occurs at temperatures as low as −196 °C. Typically only cells and tissues are subjected to cryopreservation, but biomaterials may also be used for packaging and as a cryoprotectant or cell carrier.

Increased temperature typically results in a decreased elastic modulus and strength, but increased ductility and toughness, with the opposite effects for decreased temperature. These effects are typically small for short-term exposure and small temperature differences, but can become significant near the melting temperature or glass transition temperature of a material. Long-term- or cyclic exposure to elevated temperature may result in creep of low melting temperature and viscoelastic materials, thermal degradation of polymers, increased crystallinity of polymers, or accelerated chemical degradation of materials. In general, polymers are more sensitive to temperature [157] than metals, and ceramics are least sensitive to temperature. However, select polymers such as polyphenylsulfone are routinely used for non-implantable devices subjected to more than a 1000 steam sterilization cycles without loss of mechanical properties. Hydrostatic pressure can increase the elastic modulus, strength, and more significantly, the ductility of materials, but is most likely of secondary importance relative to the effects of temperature.

Biomaterial specimens may be subjected to elevated temperature in an oven, elevated temperature and pressure in an autoclave, or low temperature in a refrigerator or freezer either continuously or cyclically prior to mechanical characterization. *In situ* testing requires a test instrument outfitted with a temperature-controlled fluid bath, oven, or environmental chamber. Environmental chambers are commercially available to facilitate *in situ* testing and thermal cycling ranging from roughly liquid nitrogen temperatures to several hundred degrees Celsius. Conditions should be carefully documented and standardized whenever possible [157].

Shape-memory alloys (e.g., Nitinol) and polymers are designed to undergo reversible changes in shape and mechanical properties (elastic modulus) upon temperature change and thus warrant special considerations for the mechanical characterization [158]. For example, Nitinol endovascular stents are designed to be easily deformed and placed into a delivery system at or below ambient temperature, but expand and exhibit superelastic properties when heated above the transformation temperature (typically 30°C) during implantation.

3.5.2. Aqueous Media

Exposure to aqueous media is generally detrimental to mechanical properties and thus used to provide a more realistic appraisal of performance in a physiological environment. Specific effects on mechanical properties are numerous and can only be introduced here. Common media utilized for mechanical

characterization of biomaterials include water, PBS, calcium-supplemented media, and FBS or synovial fluid [159–161].

Exposure to water or a humidified atmosphere may be important to characterize the effects of water uptake (swelling), interfacial degradation, and hydrolytic degradation [157,159–161]. The uptake of water in a hydrophilic biomaterial may be desirable and essential to mechanical and biological functions (e.g., soft contact lens or tissue graft). Mechanical characterization of biological tissues should always take place while fully hydrated. Hydration generally leads to decreased elastic modulus and strength, but increased ductility and toughness in such materials. For example, characterization of dehydrated collagenous tissue and scaffolds results in increased stiffness (modulus) and decreased toughness compared to characterization while hydrated [162,163]. On the other hand, the uptake of water into a synthetic biomaterial, either in bulk or at interfaces (e.g., between the matrix and fiber reinforcements), can also cause swelling or form voids that act as a precursor to mechanical failure. The combination of water uptake, corrosion, and stresses in metals can lead to stress corrosion cracking, which will be discussed further below. The combination of water uptake and stresses can lead to environmental stress crazing or cracking (ESC) in polymers and interfacial degradation in composites. Polymers and some ceramics may also intentionally (e.g., poly-α-ortho esters such as polylactide, polyglycolide and copolymers thereof, and calcium phosphates) or unintentionally degrade by hydrolysis. In polymers, ESC acts to degrade intermolecular bonds, while hydrolytic degradation degrades intramolecular bonds.

PBS provides ionic species (Na, K, Cl, and phosphates), which maintain constant pH (7.4) and more closely match levels found in the human body [159–161]. The presence of these salts can accelerate corrosion of metals. Corrosion can lead to pits and other defects that act as stress concentrations, leading to premature failure. Moreover, internal variations in stress due to applied bending, stress concentrations, and residual stresses can lead to differences in electrochemical potential, which further accelerates corrosion via galvanic corrosion. Thus, corrosion can have a profound effect on fatigue and wear such that the combined effect is much greater than either effect alone. The combination of corrosion and fatigue can eliminate the presence of a fatigue limit entirely.

Calcium-containing media is used here to describe various media containing similar salts as PBS with the addition of calcium salts. Examples include synthetic body fluid and variations of minimum essential medium (e.g., Dubecco's modified Eagle medium, DMEM), where the latter also includes various vitamins and amino acids. These media may be used to examine desirable (e.g., calcification of polymer scaffolds for bone tissue) or undesirable (e.g., calcification of cardiovascular biomaterials) calcification of biomaterials. For example, calcification of artificial and bioprosthetic heart valves occurs synergistically in highly stressed regions resulting in loss of function due to

increased biomaterial rigidity and possibly mechanical failure or thrombosis [164].

FBS provides a rich variety of proteins found in blood plasma, which may interact with biomaterial surfaces. Protein surface adsorption guides the response of cells to biomaterials, and is thus important for mechanical characterization of the interface between a biomaterial and cells/tissue in an *in vitro* or *in vivo* study. Synovial fluid provides a replication of the proteins and concentrations present in joint capsules and is thus used exclusively for simulated *in vivo* wear testing, described in Chapter 7. Protein-containing media may more accurately mimic the physiological environment, but also requires significantly greater expense and care. Without proper care, protein solutions may degrade, coagulate, or become colonized by bacteria during the course of a test, which may compromise the test entirely.

Other less common but potentially important considerations also deserve mention. Exposure to lipids may lead to swelling and degradation in otherwise stable biomaterials. For example, the fatigue properties of polysulfone were found to be degraded in the presence of lipids despite otherwise excellent mechanical properties for cardiovascular and load-bearing orthopaedic devices [165,166]. Cells and bacteria can produce an acidic microenvironment that may enhance the corrosion of metals or the degradation of some polymers and ceramics. For example, initial polyurethane insulation on pacemaker leads was highly resistant to hydrolytic degradation but often failed prematurely due to ESC initiated by direct surface oxidation mediated by a combination of host phagocytic cells and metal ions released from the conductor.

Degradation that is intended or unintended is often investigated by subjecting biomaterial samples to elevated temperature, elevated pressure, and/or aqueous media for a period of time before testing [4,157,159–161]. These tests are necessarily laborious and time intensive. Therefore, tests may be accelerated using greater than physiological levels with proper validation.

Biomaterial specimens may be subjected to any of the above aqueous media for a defined period of time prior to mechanical characterization. *In situ* testing requires a test instrument outfitted with a fluid bath or environmental chamber. Simultaneous exposure to elevated temperature and/or pressure may require a temperature-controlled fluid bath or autoclave. Sterile conditions may need to be maintained for media-containing biological molecules (e.g., DMEM or FBS). When the use of nonsubmersible transducers (e.g., clip-on extensometer) prevents the use of a fluid bath during testing, hydration may be adequately maintained over a short time period using a gravity-fed drip with a catch basin.

3.5.3. Irradiation

Sterilization by gamma or electron beam irradiation may be advantageous over steam sterilization. However, ionizing radiation can cause cross-linking or

oxidative chain scission in polymers resulting in significant, potentially deleterious, changes to mechanical properties. For example, gamma irradiation in air was discontinued for sterilization of UHMWPE orthopaedic implants due to evidence of oxidative chain scission and long-term mechanical degradation [167]. However, gamma irradiation has also been used to cross-link UHMWPE for improved wear resistance, but highly cross-linked UHMWPE incurs a loss of tensile strength, ductility, toughness, and fatigue resistance [168]. Due to the long-term nature of irradiation damage, accelerated aging conditions are often utilized prior to mechanical characterization.

3.6. DATA ACQUISITION AND ANALYSIS

When acquiring signals from transducers (e.g., load cell, LVDT, extensometer, etc.) for either data collection or system control [48,49], the appropriate *data acquisition rate* and *bandwidth* should consider the strain rate, loading frequency, and material behavior. The bandwidth reflects the frequency sensitivity. As a general guideline, the data acquisition rate should not exceed 10-times the bandwidth. An excessive data acquisition rate (oversampling) and bandwidth can result in unnecessary data and noise, respectively. A low data acquisition rate (undersampling) and bandwidth can result in the loss or filtering of meaningful data (e.g., peaks) and potentially incorrect results. For example, a split Hopkinson bar test for high strain rate testing typically requires a frequency response of 100 kHz [86].

Nearly all modern digital control and data acquisition systems include user-friendly *software* enabling the creation of custom test methods, automatic calculation of mechanical properties, and generation of reports. However, these advantages can also cause problems if a negligent user is not aware that the wrong data are being used for the calculation of a mechanical property. Unfortunately, I've consulted for a client only to determine that a previous "professional" consulting firm hired to provide accurate data had made this egregious error. The moral of the story is that one must take care and responsibility for all that is happening "behind" the user interface window. Computers and software have not yet replaced the importance of a knowledgeable and skilled test engineer!

Data analysis for the mechanical characterization of biomaterials can be greatly aided by a few basic *statistical methods* [169,170]. Force-displacement or stress–strain data can be fit using *linear or nonlinear least squares regression*. The correlation coefficient (R^2) provides a measure of the goodness of fit. Biological systems and interactions with biological systems generally produce greater variability than most engineering systems. Therefore, *analysis of variance* (ANOVA) or regression models should be used to examine whether an experimental factor (or variable) exhibits a statistically significant influence on a mechanical property. The criteria for significance are (by convention) taken at a level of 95% confidence or a p-value less than 0.05. Interactions between

multiple factors and their relative influence can also be considered statistically using these methods. In the case of grouped data, post hoc comparisons should be used after ANOVA has determined that a factor is significant. The *t*-test is most common, although Tukey's HSD test is considered more conservative. These tests assume that the data are normally distributed. Therefore, data exhibiting a non-normal distribution or an unknown distribution due to a small sample size are best examined using nonparametric methods (e.g., Kruskal–Wallis ANOVA and Wilcoxon post hoc tests).

ANOVA and post hoc tests indicate whether an effect or difference is statistically significant, but note that statistical equivalence is an entirely different matter and should not be claimed. Additionally, in tests where the measured effect of a variable or the difference between two groups is not statistically significant, further testing and analysis may be required. Retrospective *power analysis* using the test data can determine whether an effect or difference could have been measured using a greater sample size and the number of additional samples needed. The claim that an effect or difference is "not statistically significant" can only be made when the *p*-value is greater than the level of significance and the statistical power is sufficiently high (sometimes taken as greater than 0.80). A prospective power analysis can be extremely useful in the design of experiments when possible. Given reasonable estimates of the difference to be detected, error standard deviation, and level of significance, the statistical power of various sample sizes can be estimated.

Thorough statistical analysis often requires methods and capabilities beyond what is available in test instrument control and data acquisition packages. A number of software packages are commercially available or open source, ranging from products that are very powerful and comprehensive (e.g., SAS, SPSS, R, Matlab) to more user friendly (e.g., JMP, GraphPad, AcaStat). Specific packages and modules are also available for Weibull analysis, fatigue crack propagation, and other methods.

ACKNOWLEDGMENTS

This chapter was made possible by 40 years of learning facilitated by federal and private funding, which has supported my research, clients who trust my judgment, students who teach me more than I could ever learn on my own, colleagues who constantly sharpen my skills, professional and personal mentors who encouraged me to pursue my career path, college and graduate school instructors who introduced me to the mechanical behavior of materials, manual mechanically-oriented labor that taught the necessity of hard work and motivated study, and parents who encouraged youthful curiosity. Words cannot express my gratitude for the constant love and support of my wife Lisa, and children Zachary and Eliana. Finally, this chapter was also made possible by the ordered complexity of condensed matter (a.k.a., the science of materials) and the laws of mechanics, which are ignored only at great personal and societal risk!

REFERENCES

[1] Sumner DR, Turner TM, Igloria R, Urban RM, Galante JO. Functional adaptation and ingrowth of bone vary as a function of hip implant stiffness. J Biomech 1998;31:909–17.

[2] Neumann A, Jahnke K. Biomaterials for ossicular chain reconstruction. A Review. Mat wiss u Werkstofftech 2003;34:1052–7.

[3] Nicolson PC, Vogt J. Soft contact lens polymers: an evolution. Biomaterials 2001;22:3273–83.

[4] Middleton JC, Tipton AJ. Synthetic biodegradable polymers as orthopedic devices. Biomaterials 2000;21:2335–46.

[5] Pruitt LA, Chakravartula AM. Mechanics of biomaterials. Cambridge, UK: Cambridge University Press; 2011.

[6] Bowman K. Mechanical behavior of materials. John Wiley and Sons, Inc; 2004.

[7] Dowling NE. Mechanical behavior of materials. Upper Saddle River, NJ: Pearson Prentice Hall; 2012.

[8] Meyers MA, Chawla KK. Mechanical behavior of materials. Cambridge, UK: Cambridge University Press; 2008.

[9] McAfee OC. Interbody fusion cages in reconstructive operations on the spine. J Bone Joint Surg 1999;81A:859–80.

[10] Vadapalli S, Sairyo K, Goel VK, Robon M, Biyani A, Khandha A, et al. Biomechanical rationale for using polyetheretherketone (PEEK) spacers for lumbar interbody fusion – a finite element study. Spine 2006;31:E992–8.

[11] Roeder RK, Smith SM, Conrad TL, Yanchak NJ, Merrill CH, Converse GL. Porous and bioactive PEEK implants for interbody spinal fusion. Adv Mater Process 2009;167:46–8.

[12] ASTM D638-01. Standard test method for tensile properties of plastics. West Conshohocken, PA: American Society for Testing and Materials; 2001.

[13] Chawla KK. Composite materials science and engineering. 2nd ed. New York, NY: Springer; 1998.

[14] Halpin JC. Primer on composite materials analysis. 2nd ed. Lancaster, PA: Technomic Publishing Co; 1992.

[15] Hinchliffe A. Molecular modeling for beginners. 2nd ed. Chichester, UK: John Wiley and Sons Ltd; 2011.

[16] Holzapfel GA. Nonlinear solid mechanics: a continuum approach for engineering. Chichester, UK: John Wiley and Sons Ltd; 2000.

[17] Hollingsworth NT, Wagner DR. Modeling shear behavior of the annulus fibrosus. J Mech Behav Biomed Mater 2011;4:1103–14.

[18] Vincent JFV. Survival of the cheapest. Mater Today 2002;5:28–41.

[19] Chen P-Y, Lin AYM, Lin Y-S, Seki Y, Stokes AG, Peyras J, et al. Structural and mechanical properties of selected biological materials. J Mech Behav Biomed Mater 2008;1:208–26.

[20] Gordon JE. The new science of strong materials. Princeton, NJ: Princeton University Press; 1976.

[21] Pilkey WD, Pilkey DF. Peterson's stress concentration factors. Hoboken, NJ: John Wiley and Sons, Inc; 2008.

[22] Griffith AA. The phenomena of rupture and flow in solids. Phil Trans R Soc 1920; 221A:163–98.

[23] Anderson TL. Fracture mechanics: fundamentals and applications. 3rd ed. Boca Raton, FL: Taylor and Francis Group; 2005.

[24] Sun CT, Jin Z-H. Fracture mechanics. Waltham, MA: Academic Press; 2012.

[25] Tada H, Paris PC, Irwin GR. The stress analysis of cracks handbook. 3rd ed. New York, NY: American Society of Mechanical Engineers; 2000.
[26] Murakami Y. Stress intensity factors handbook. New York, NY: Pergamon Press; 1987.
[27] ASTM E399-09. Standard test method for linear-elastic plane-strain fracture toughness K_{Ic} of metallic materials. West Conshohocken, PA: American Society for Testing and Materials; 2009.
[28] ASTM C1421-10. Standard test method for determination of fracture toughness of advanced ceramics at ambient temperature. West Conshohocken, PA: American Society for Testing and Materials; 2010.
[29] Zimmermann EA, Barth HD, Ritchie RO. The multiscale origins of fracture resistance in human bone and its biological degradation. JOM 2012;64:486–93.
[30] ASTM E1290-08. Standard test method for crack-tip opening displacement (CTOD) fracture toughness measurement. West Conshohocken, PA: American Society for Testing and Materials; 2008.
[31] ASTM E1820-11. Standard test method for measurement of fracture toughness. West Conshohocken, PA: American Society for Testing and Materials; 2011.
[32] Ritchie RO, Koester KJ, Ionova S, Yao W, Lane NE, Ager III JW. Measurement of the toughness of bone: a tutorial with special reference to small animal studies. Bone 2008;43:798–812.
[33] Taylor D, Kuiper J-H. The prediction of stress fractures using a stressed volume concept. J Orthop Res 2001;19:919–26.
[34] Creyke WEC, Sainsbury IEJ, Morrell R. Design with non-ductile materials. New York, NY: Applied Science Publishers; 1982.
[35] ASTM C1239-07. Standard test method for reporting uniaxial strength data and estimating Weibull distribution parameters for advanced ceramics. West Conshohocken, PA: American Society for Testing and Materials; 2007.
[36] ASTM C1683-10. Standard test method for size scaling of tensile strengths using Weibull statistics for advanced ceramics. West Conshohocken, PA: American Society for Testing and Materials; 2010.
[37] Turner CH, Roeder RK, Wieczorek A, Foroud T, Liu G, Peacock M. Variability in skeletal mass, structure, and biomechanical properties among inbred strains of rats. J Bone Miner Res 2001;16:1532–9.
[38] Oberg E. Machinery's handbook. 28th ed. New York, NY: Industrial Press; 2008.
[39] Davis JR. Metals handbook. In: Machining, vol. 16. Materials Park, OH: ASM International; 1989.
[40] Marinescu ID. Handbook of advanced ceramics machining. Boca Raton, FL: CRC Press; 2006.
[41] ASTM D3641-12. Standard practice for injection molding test specimens of thermoplastic molding and extrusion materials. West Conshohocken, PA: American Society for Testing and Materials; 2012.
[42] ASTM F451-08. Standard specification for acrylic bone cement. West Conshohocken, PA: American Society for Testing and Materials; 2008.
[43] Kalpakjian S, Schmid SR. Manufacturing processes for engineering materials. 5th ed. Upper Saddle River, NJ: Pearson Education; 2008.
[44] ASTM C1161-02. Standard test method for flexural strength of advanced ceramics at ambient temperature. West Conshohocken, PA: American Society for Testing and Materials; 2002.
[45] ASTM E4-10. Standard test method for force verification of testing machines. West Conshohocken, PA: American Society for Testing and Materials; 2010.

[46] ASTM E251-92. Standard test methods for performance characteristics of metallic bonded resistance strain gages. West Conshohocken, PA: American Society for Testing and Materials; 2009.
[47] Shelton JC, Orr JF, editors. Optical measurement methods in biomechanics. London, UK: Chapman and Hall; 1996.
[48] Dunn PF. Measurement and data analysis for engineering and science. 2nd ed. Boca Raton, FL: CRC Press; 2010.
[49] Morris AS, Langari R. Measurement and instrumentation: theory and application. Waltham, MA: Academic Press; 2011.
[50] Davis JR. Tensile testing. 2nd ed. Materials Park, OH: ASM International; 2004.
[51] ISO 11405. Testing of adhesion to tooth structure. International organization for standardization. Geneva: Switzerland; 2003.
[52] Sano H, Shono T, Sonoda H, Takatsu T, Ciucchi B, Carvalho R, et al. Relationships between surface area for adhesion and tensile bond strength – evaluation of a micro-tensile bond test. Dent Mater 1994;10:236–40.
[53] ASTM C1424-10. Standard test method for monotonic compressive strength of advanced ceramics at ambient temperature. West Conshohocken, PA: American Society for Testing and Materials; 2010.
[54] ASTM D695-10. Standard test method for compressive properties of rigid plastics. West Conshohocken, PA: American Society for Testing and Materials; 2010.
[55] ASTM D1621-10. Standard test method for compressive properties of rigid cellular plastics. West Conshohocken, PA: American Society for Testing and Materials; 2010.
[56] Gibson LJ, Ashby MF. Cellular solids: structure and properties. Cambridge, UK: Cambridge University Press; 2001.
[57] Sacks MS, Sun W. Multiaxial mechanical behavior of biological materials. Annu Rev Biomed Eng 2003;5:251–84.
[58] Hollingsworth NT, Wagner DR. The stress and strain states of the posterior annulus fibrosus under flexion. Spine 2012;37:E1134–9.
[59] Roeder R, Wolfe J, Lianakis N, Hinson T, Geddes LA, Obermiller J. Compliance, elastic modulus, and burst pressure of small-intestine submucosa (SIS), small-diameter vascular grafts. J Biomed Mater Res 1999;47:65–70.
[60] Jaekel DJ, MacDonald DW, Kurtz SM. Characterization of PEEK biomaterials using the small punch test. J Mech Behav Biomed Mater 2011;4:1275–82.
[61] ASTM F2183-02. Standard test method for small punch testing of ultra-high molecular weight polyethylene used in surgical implants. West Conshohocken, PA: American Society for Testing and Materials; 2002.
[62] ASTM F543-07. Standard specification and test methods for metallic medical bone screws. West Conshohocken, PA: American Society for Testing and Materials; 2007.
[63] Reilly DT, Burstein AH. The elastic and ultimate properties of compact bone tissue. J Biomech 1975;8:393–405.
[64] Dong XN, Guo XE. The dependence of transversely isotropic elasticity of human femoral cortical bone on porosity. J Biomech 2004;37:1281–7.
[65] ASTM C496-11. Standard test method for splitting tensile strength of cylindrical concrete specimens. West Conshohocken, PA: American Society for Testing and Materials; 2011.
[66] Procopio AT, Zavaliangos A, Cunningham JC. Analysis of the diametral compression test and the applicability to plastically deforming materials. J Mater Sci 2003;38:3629–39.
[67] Pittet C, Lemaître J. Mechanical characterization of brushite cements: a Mohr circles' approach. J Biomed Mater Res Appl Biomater 2000;53:769–80.

[68] Ferracane JL, Greener EH. The effect of resin formulation on the degree of conversion and mechanical properties of dental restorative resins. J Biomed Mater Res 1986;20:121–31.
[69] Gere JM, Goodno BJ. Mechanics of materials. 8th ed. Stamford, CT: Cengage Learning; 2013.
[70] ASTM D790-10. Standard test methods for flexural properties of unreinforced and reinforced plastics and electrical insulating materials. West Conshohocken, PA: American Society for Testing and Materials; 2010.
[71] ASTM D6272-10. Standard test method for flexural properties of unreinforced and reinforced plastics and electrical insulating materials by four-point bending. West Conshohocken, PA: American Society for Testing and Materials; 2010.
[72] ASTM D5379-05. Standard test method for shear properties of composite materials by V-notched beam method. West Conshohocken, PA: American Society for Testing and Materials; 2005.
[73] Lee S, Munro M. Evaluation of in-plane shear test methods for advanced composite materials by the decision analysis technique. Composites 1986;17:13–22.
[74] Adams DF. A comparison of shear test methods. High Perform Compos, www.compositesworld.com September 2005.
[75] Turner CH, Wang T, Burr DB. Shear strength and fatigue properties of human cortical bone determined from pure shear tests. Calcif Tissue Int 2001;69:373–8.
[76] An YH, Draughn RA. Mechanical testing of bone and the bone-implant. Boca Raton, FL: Interface CRC Press; 2000.
[77] Dhert WJA, Verheyen CCPM, Braak LH, de Wijn JR, Klein CPAT, de Groot K, et al. A finite element analysis of the push-out test: influence of test conditions. J Biomed Mater Res 1992;26A:119–30.
[78] Berzins A, Shah B, Weinans H, Sumner DR. Nondestructive measurements of implant-bone interface shear modulus and effects of implant geometry in pull-out tests. J Biomed Mater Res 1997;34A:337–40.
[79] Siewert TA, Manahan Sr. MP, editors. Pendulum impact testing: a century of progress. STP 1380. West Conshohocken, PA: American Society for Testing and Materials; 2000.
[80] ASTM E23-07. Standard test methods for determining the notched bar impact testing of metallic materials. West Conshohocken, PA: American Society for Testing and Materials; 2007.
[81] ASTM D256-10. Standard test methods for determining the Izod pendulum impact resistance of plastics. West Conshohocken, PA: American Society for Testing and Materials; 2010.
[82] ASTM D6110-10. Standard test methods for determining the Charpy impact resistance of notched specimens of plastics. West Conshohocken, PA: American Society for Testing and Materials; 2010.
[83] ASTM D5420-10. Standard test method for impact resistance of flat, rigid plastic specimen by means of a striker impacted by a falling weight (Gardner impact). West Conshohocken, PA: American Society for Testing and Materials; 2010.
[84] ASTM D1709-09. Standard test methods for impact resistance of plastic film by the free falling dart method. West Conshohocken, PA: American Society for Testing and Materials; 2009.
[85] Mott PH, Twigg JN, Roland DF, Schrader HS, Pathak JA, Roland CM. High-speed tensile test instrument. Rev Sci Instrum 2007;78:045105.
[86] Chen W, Song B. Split Hopkinson (Kolsky) bar design, testing and applications. New York, NY: Springer; 2010.

[87] Meyers MA. Dynamic behavior of materials. New York, NY: John Wiley and Sons; 1994.
[88] Ravi-Chandar K. Dynamic fracture. Amsterdam, The Netherlands: Elsevier; 2004.
[89] Kulin RM, Jiang F, Vecchio KS. Effects of age and loading rate on equine cortical bone failure. J Mech Behav Biomed Mater 2011;4:57–75.
[90] Pilcher A, Wang X, Kaltz Z, Garrison JG, Niebur GL, Mason J, et al. High strain rate testing of bovine trabecular bone. J Biomech Eng 2011;132:081012. p. 7.
[91] ASTM E2448-11. Standard test method for determining the superplastic properties of metallic sheet materials. West Conshohocken, PA: American Society for Testing and Materials; 2011.
[92] ASTM E2712-09. Standard test methods for forming superplastic metallic sheet. West Conshohocken, PA: American Society for Testing and Materials; 2009.
[93] ASTM E139-11. Standard test methods for conducting creep, creep-rupture, and stress-rupture tests of metallic materials. West Conshohocken, PA: American Society for Testing and Materials; 2011.
[94] ASTM C1291-00. Standard test method for elevated temperature tensile creep strain, creep strain rate, and creep time-to-failure for advanced monolithic ceramics. West Conshohocken, PA: American Society for Testing and Materials; 2010.
[95] ASTM D2990-09. Standard test methods for tensile, compressive, and flexural creep and creep-rupture of plastics. West Conshohocken, PA: American Society for Testing and Materials; 2009.
[96] Ward IM, Sweeney J. The mechanical properties of solid polymers. 2nd ed. Chichester, UK: John Wiley and Sons; 2004.
[97] Shepherd TN, Zhang J, Ovaert TO, Roeder RK, Niebur GL. Direct comparison of nano-indentation and macroscopic measurements of bone viscoelasticity. J Mech Behav Biomed Mater 2011;4:2055–62.
[98] ASTM E328-02. Standard test methods for stress relaxation for materials and structures. West Conshohocken, PA: American Society for Testing and Materials; 2008.
[99] ASTM D6048-07. Standard practice for stress relaxation testing of raw rubber, unvulcanized rubber compounds, and thermoplastic elastomers. West Conshohocken, PA: American Society for Testing and Materials; 2007.
[100] ASTM E467-08. Standard practice for verification of constant amplitude dynamic forces in an axial fatigue testing system. West Conshohocken, PA: American Society for Testing and Materials; 2008.
[101] ASTM E1942-98. Standard guide for evaluating data acquisition systems used in cyclic fatigue and fracture mechanics testing. West Conshohocken, PA: American Society for Testing and Materials; 2010.
[102] ASTM C1361-10. Standard practice for constant amplitude, axial, tension-tension cyclic fatigue of advanced ceramics at ambient temperature. West Conshohocken, PA: American Society for Testing and Materials; 2010.
[103] ASTM F2118-10. Standard test method for constant amplitude of force controlled fatigue testing of acrylic bone cement materials. West Conshohocken, PA: American Society for Testing and Materials; 2010.
[104] ASTM E466-07. Standard practice for conducting force controlled constant amplitude axial fatigue tests of metallic materials. West Conshohocken, PA: American Society for Testing and Materials; 2007.
[105] ASTM E468-11. Standard practice for presentation of constant amplitude fatigue test results for metallic materials. West Conshohocken, PA: American Society for Testing and Materials; 2011.
[106] ASTM D7791-12. Standard test method for uniaxial fatigue properties of plastics. West Conshohocken, PA: American Society for Testing and Materials; 2012.

[107] ASTM D3479-96. Standard test method for tension-tension fatigue of polymer matrix composite materials. West Conshohocken, PA: American Society for Testing and Materials; 2007.
[108] ASTM E606-04. Standard practice for strain-controlled fatigue testing. West Conshohocken, PA: American Society for Testing and Materials; 2004.
[109] Cook SD, Georgette FS, Skinner HB, Haddad Jr RJ. Fatigue properties of carbon- and porous-coated Ti-6Al-4V alloy. J Biomed Mater Res 1984;18:497–512.
[110] ASTM D7774-12. Standard test method for flexural fatigue properties of plastics. West Conshohocken, PA: American Society for Testing and Materials; 2012.
[111] Kane RJ, Converse GL, Roeder RK. Effects of the reinforcement morphology on the fatigue properties of hydroxyapatite reinforced polymers. J Mech Behav Biomed Mater 2008;1:261–8.
[112] Landrigan MD, Roeder RK. Systematic error in mechanical measures of damage during four-point bending fatigue of cortical bone. J Biomech 2009;4:1212–7.
[113] ASTM F2477-07. Standard test methods for in vitro pulsatile durability testing of vascular stents. West Conshohocken, PA: American Society for Testing and Materials; 2007.
[114] Pelton AR, Schroeder V, Mitchell MR, Gong X-Y, Barney M, Robertson SW. Fatigue and durability of nitinol stents. J Mech Behav Biomed Mater 2008;1:153–64.
[115] Runciman A, Xu D, Pelton AR, Ritchie RO. An equivalent strain/Coffin-Manson approach to multiaxial fatigue and life prediction in superelastic Nitinol medical devices. Biomaterials 2011;32:4987–93.
[116] ASTM E739-10. Standard practice for statistical analysis of linear or linearized stress-life (*S-N*) and strain-life (ε-*N*) fatigue data. West Conshohocken, PA: American Society for Testing and Materials; 2010.
[117] Kane RJ, Yue W, Mason JJ, Roeder RK. Improved fatigue life of acrylic bone cements reinforced with zirconia fibers. J Mech Behav Biomed Mater 2010;3:504–11.
[118] Niinomi M. Mechanical biocompatibilities of titanium alloys for biomedical applications. J Mech Behav Biomed Mater 2008;1:30–42.
[119] Sobieraj MC, Murphy JE, Brinkman JG, Kurtz SM, Rimnac CM. Notched fatigue behavior of PEEK. Biomaterials 2010;31:9156–62.
[120] Pattin CA, Caler WE, Carter DR. Cyclic mechanical property degradation during fatigue loading of cortical bone. J Biomech 1996;29:69–79.
[121] Cotton JR, Winwood K, Zioupos P, Taylor M. Damage rate is a predictor of fatigue life and creep strain rate in tensile human cortical bone samples. J Biomech Eng 2005;127:213–9.
[122] Cotton JR, Zioupos P, Winwood K, Taylor M. Analysis of creep strain during tensile fatigue of cortical bone. J Biomech 2003;36:943–9.
[123] ASTM E2714-09. Standard test method for creep-fatigue testing. West Conshohocken, PA: American Society for Testing and Materials; 2009.
[124] ASTM E647-11. Standard test method for measurement of fatigue crack growth rates. West Conshohocken, PA: American Society for Testing and Materials; 2011.
[125] Connors WC. Fatigue striation spacing analysis. Mater Char 1994;33:245–53.
[126] Bajaj D, Sundaram N, Arola D. An examination of fatigue striations in human dentin: in vitro and in vivo. J Biomed Mater Res 2008;85B:149–59.
[127] ASTM E2760-10. Standard test method for creep-fatigue crack growth testing. West Conshohocken, PA: American Society for Testing and Materials; 2010.
[128] Menard KP. Dynamic mechanical analysis. 2nd ed. Boca Raton, FL: CRC Press; 2008.
[129] ASTM D4065-06. Standard practice for plastics: dynamic mechanical properties: determination and report of procedures. West Conshohocken, PA: American Society for Testing and Materials; 2006.

[130] Hellier CJ. Handbook of nondestructive evaluation. New York, NY: McGraw-Hill; 2001.
[131] Herrmann K. Hardness testing: principles and applications. Materials Park, OH: ASM International; 2011.
[132] ASTM E10-12. Standard test method for Brinell hardness of metallic materials. West Conshohocken, PA: American Society for Testing and Materials; 2012.
[133] ASTM E18-11. Standard test methods for Rockwell hardness of metallic materials. West Conshohocken, PA: American Society for Testing and Materials; 2011.
[134] ASTM D785-08. Standard test method for Rockwell hardness of plastics and electrical insulating materials. West Conshohocken, PA: American Society for Testing and Materials; 2008.
[135] ASTM E140-07. Standard hardness conversion tables for metals: relationship among Brinell hardness, Vickers hardness, Rockwell hardness, Superficial hardness, Knoop hardness, and Scleroscope hardness. West Conshohocken, PA: American Society for Testing and Materials; 2007.
[136] ASTM E384-11. Standard test method for Knoop and Vickers hardness of materials. West Conshohocken, PA: American Society for Testing and Materials; 2011.
[137] ASTM C1326-08. Standard test method for Knoop indentation hardness of advanced ceramics. West Conshohocken, PA: American Society for Testing and Materials; 2008.
[138] ASTM C1327-08. Standard test method for Vickers indentation hardness of advanced ceramics. West Conshohocken, PA: American Society for Testing and Materials; 2008.
[139] Oliver WC, Pharr GM. Measurement of hardness and elastic modulus by instrumented indentation: advances in understanding and refinements to methodology. J Mater Res 2004;19:3–20.
[140] Fischer-Cripps AC. Nanoindentation. 3rd ed. New York, NY: Springer; 2011.
[141] Ebenstein DM, Pruitt LA. Nanoindentation of biological materials. Nano Today 2006;1:26–33.
[142] ASTM D2240-05. Standard test method for rubber property–durometer hardness. West Conshohocken, PA: American Society for Testing and Materials; 2010.
[143] Slaboch CL, Alber MS, Rosen ED, Ovaert TO. Mechano-rheological properties of the murine thrombus determined via nanoindentation and finite element modeling. J Mech Behav Biomed Mater 2012;10:75–86.
[144] Blum MM, Ovaert TC. A novel polyvinyl alcohol hydrogel functionalized with organic boundary lubricant for use a low-friction cartilage substitute: synthesis, physical/chemical, mechanical, and friction characterization. J Biomed Mater Res 2012;100B:1755–63.
[145] Kruzic JJ, Kim DK, Koester KJ, Ritchie RO. Indentation techniques for evaluating the fracture toughness of biomaterials and hard tissues. J Mech Behav Biomed Mater 2009;2:384–95.
[146] Anstis GR, Chantikul P, Lawn BR, Marshall DB. A critical evaluation of indentation techniques for measuring fracture toughness: I, direct crack measurements. J Am Ceram Soc 1981;64:533–8.
[147] Marshall DB, Noma T, Evans AG. A simple method for determining elastic-modulus-to-hardness ratios using Knoop indentation measurements. J Am Ceram Soc 1982;65:C175–6.
[148] Ensminger D, Bond LJ. Ultrasonics: fundamentals, technology, and applications. 3rd ed. Boca Raton, FL: CRC Press; 2011.
[149] Van Buskirk WC, Cowin SC, Ward RN. Ultrasonic measurement of orthotropic elastic constants of bovine femoral bone. J Biomech Eng 1981;103:67–72.
[150] Ashman RB, Cowin SC, Van Buskirk WC, Rice JC. A continuous wave technique for the measurement of the elastic properties of cortical bone. J Biomech 1984;17:349–61.

[151] Kohles SS, Bowers JR, Vailas AC, Vanderby Jr R. Ultrasonic wave velocity measurement in small polymeric and cortical bone specimens. J Biomech Eng 1997;119:232–6.
[152] Espinoza Orías AA, Deuerling JM, Landrigan MD, Renaud JE, Roeder RK. Anatomic variation in the elastic anisotropy of cortical bone tissue in the human femur. J Mech Behav Biomed Mater 2009;2:255–63.
[153] Hofmann T, Heyroth F, Meinhard H, Franzel W, Raum K. Assessment of composition and anisotropic elastic properties of secondary osteon lamellae. J Biomech 2006;39:2282–94.
[154] Bhardwaj MC. High-resolution ultrasonic characterization. Ceram Bull 1990;69:1490–6.
[155] ASTM C373-88. Standard test method for water absorption, bulk density, apparent porosity, and apparent specific gravity of fired Whiteware products. West Conshohocken, PA: American Society for Testing and Materials; 2006.
[156] ASTM D792-08. Standard test methods for density and specific gravity (relative density) of plastics by displacement. West Conshohocken, PA: American Society for Testing and Materials; 2008.
[157] ASTM D618-08. Standard practice of conditioning plastics for testing. West Conshohocken, PA: American Society for Testing and Materials; 2008.
[158] ASTM F2516-07. Standard test method for tension testing of nickel-titanium superelastic materials. West Conshohocken, PA: American Society for Testing and Materials; 2007.
[159] ASTM F1634-95. Standard practice for in-vitro environmental conditioning of polymer matrix composite materials and implants. West Conshohocken, PA: American Society for Testing and Materials; 2008.
[160] ASTM F1635-11. Standard test method for in vitro degradation testing of hydrolytically degradable polymer resins and fabricated forms for surgical implants. West Conshohocken, PA: American Society for Testing and Materials; 2011.
[161] ASTM F2150-07. Standard guide for characterization and testing of biomaterial scaffolds used in tissue-engineered medical products. West Conshohocken, PA: American Society for Testing and Materials; 2007.
[162] Nyman JS, Roy A, Shen X, Acuna RL, Tyler JH, Wang X. The influence of water removal on the strength and toughness of cortical bone. J Biomech 2006;39:931–8.
[163] Harley BA, Leung JH, Silva ECCM, Gibson LJ. Mechanical characterization of collagen-glycosaminoglycan scaffolds. Acta Biomaterialia. 2007;3:463–74.
[164] Schoen FJ, Levy RJ. Calcification of tissue heart valve substitutes: progress toward understanding and prevention. Ann Thorac Surg 2005;79:1072–80.
[165] Asgian CM, Gilbertson LN, Blessing NN, Crowninshield RD. Environmentally induced fracture of polysulfone in lipids. Trans. of the 15th annual meeting of the society for biomaterials. Birmingham, AL, 17; 1989.
[166] Trentacosta JD, Cheban JC. Lipid sensitivity of polyaryl-ether-ketones and polysulfone. Trans Orthop Res Soc 1995;41:783.
[167] Kurtz SM, Muratoglu OK, Evans M, Edidin AA. Advances in the processing, sterilization, and crosslinking of ultra-high molecular weight polyethylene for total joint arthroplasty. Biomaterials 1999;20:1659–88.
[168] Pruitt LA. Deformation, yielding, fracture and fatigue behavior of conventional and highly cross-linked ultra high molecular weight polyethylene. Biomaterials 2005;26:905–15.
[169] NIST/SEMATECH e-Handboook of Statistical Methods. National Institute of Standards and Technology. Gaithersberg, MD, http://www.itl.nist.gov/div898/handbook/; 2012.
[170] McKillup S. Statistics explained: an introductory guide for life scientists. Cambridge, UK: Cambridge University Press; 2005.